Effect of impurities on grain growth in cold ice sheets

G. Durand,[1,2] J. Weiss,[1] V. Lipenkov,[3] J. M. Barnola,[1] G. Krinner,[1] F. Parrenin,[1] B. Delmonte,[1] C. Ritz,[1] P. Duval,[1] R. Röthlisberger,[4,5] and M. Bigler[2,4]

Received 4 April 2005; revised 13 October 2005; accepted 16 November 2005; published 4 March 2006.

[1] On the basis of a detailed study of the ice microstructure of the European Project for Ice Coring in Antarctica (EPICA) ice core at Dome Concordia, Antarctica, we analyze the effect of impurities (solubles, and insolubles, that is, dust particles) on the grain growth process in cold ice sheets. As a general trend, the average grain size increases with depth. This global increase, induced by the normal grain growth process, is punctuated by several sharp decreases that can be associated with glacial-interglacial climatic transitions. To explain the modifications of the microstructure with climatic changes, we discuss the role of soluble and insoluble impurities on the grain growth process, coupled with an analysis of the pinning of grain boundaries by microparticles. Our data indicate that high soluble impurity content does not necessarily imply a slowdown of grain growth kinetics, whereas the pinning of grain boundaries by dust explains all the observed modifications of the microstructure. We propose a numerical model of the evolution of the average grain size in deep ice cores that takes into account recrystallization processes such as normal grain growth and rotation recrystallization as well as the pinning effect induced by dust particles, bubbles, and clathrates on the grain boundaries. Applied to the first 2135 m of the Dome Concordia core, the model reproduces accurately the measured mean grain radius. This indicates a major role of dust in the modification of polar ice microstructure and shows that the average grain size is not a true paleothermometer, as it is correlated with climatic transitions through the dust content of the ice.

Citation: Durand, G., et al. (2006), Effect of impurities on grain growth in cold ice sheets, *J. Geophys. Res.*, *111*, F01015, doi:10.1029/2005JF000320.

1. Introduction

[2] Deep drilling within cold ice sheets is an extraordinary tool for paleoclimatic studies. Even though traditionally most of the information on paleoclimate comes from water isotopes and chemical analyses, the study of ice microstructure (grain sizes and grain shapes) is of great interest. Indeed, the microstructure controls many physical properties of the ice [*Alley et al.*, 1986a], the grain size could have an effect on the ice sheet strain rate [*Cuffey et al.*, 2000], and the microstructure can record the past deformation [*Durand et al.*, 2004] or the climatic history.

[3] In the nearly isothermal upper part of cold ice sheets corresponding to Holocene ice, the average grain size increases with depth [*Alley et al.*, 1986a; *Gow*, 1969]: this is the normal grain growth process driven by a reduction in the total grain boundary energy within the material [see, e.g., *Ralph*, 1990; *Humphreys and Hatherly*, 1996] for a general introduction on grain growth in polycrystalline materials). However, *Duval and Lorius* [1980] observed a sharp decrease of the average grain size associated to the climatic transition Holocene–Last Glacial Maximum (LGM) along the first Dome C ice core. Since then, several explanations have been proposed to explain this correlation between grain size and climate, including drag on grain boundary migration by soluble impurities [*Alley and Woods*, 1996], pinning by (insoluble) microparticles [*Fisher and Koerner*, 1986; *Gow et al.*, 1997; *Jun et al.*, 1998], or an effect of surface temperature conditions at the time of deposition [*Petit et al.*, 1987]. However, because many parameters, including isotopic record, conductivity, concentrations of different soluble impurities or of dust particles, together exhibit abrupt changes at climatic transitions, it seems difficult to determine the correct mechanism only on the basis of correlations between the average grain size and these parameters.

[4] During the last 30 years, most of the studies on polar ice microstructure focused on the evolution of the average grain size with depth, and so age. This average grain size was generally determined by manual counting on 2D thin sections of ice, a tedious and time consuming process. Today, image analysis allows an automatic extraction of

[1]Laboratoire de Glaciologie et Géophysique de l'Environnement, CNRS and Université Joseph Fourier, Saint-Martin-d'Heres, France.
[2]Now at Niels Bohr Institute, University of Copenhagen, Copenhagen, Denmark.
[3]Arctic and Antarctic Research Institute, St. Petersburg, Russia.
[4]Climate and Environmental Physics, University of Bern, Bern, Switzerland.
[5]Now at British Antarctic Survey, Cambridge, UK.

0148-0227/06/2005JF000320$09.00

the microstructure (the grain boundaries, noted as GB in what follows) from 2D thin sections [*Gay and Weiss*, 1999]. This improves the accuracy of the estimation of the average grain size (better statistics), and allows the determination of other microstructural characteristics such as grain size distributions, grain shape anisotropy [*Arnaud et al.*, 2000], or even the strain tensor recorded by the microstructure [*Durand et al.*, 2004]. In this paper, we analyze the grain growth process in cold ice sheets and the effect of impurities (solubles and insolubles) in the light of such detailed studies of the microstructure. Other recrystallization processes take place in polar ice, such as rotation and migration recrystallization [*De La Chapelle et al.*, 1998]. Induced by deformation, these mechanisms do not significantly affect the ice microstructure in shallow ice. Migration recrystallization, which results from the rapid migration of GB between dislocation-free nuclei and deformed grains, occurs only at temperatures above $-10°C$ [*Duval and Castelnau*, 1995] corresponding to depths below 2925 m for the European Project for Ice Coring in Antarctica (EPICA) Dome Concordia ice core analyzed here, that is, much below the explored depth range (100–2200 m). Rotation recrystallization is characterized by basal dislocations that group together in walls perpendicular to slip planes to form subboundaries. In the end, this process leads to the division of old grains into smaller grains, that is, decreases the average grain size. In the Byrd ice core of Antarctica, this process is strong enough to fully balance grain growth from the depth of 400 m [*Alley et al.*, 1995]; in the GRIP ice core of Greenland, the depth is 650 m [*Thorsteinsson et al.*, 1997]). On the other hand, the average grain size increases at least down to 2500 m along the Vostok ice core (Antarctica), showing that rotation recrystallization is unable to balance grain growth down to this depth [*Duval and Castelnau*, 1995]. As shown in this paper, the same result is observed for the EPICA ice core.

[5] This work is based mainly on an analysis of the EPICA ice core at Dome Concordia, Antarctica. The paper is organized as follows: in section 2, we recall the classical models of grain growth in polycrystalline materials and the effects of impurities that are essential for the forthcoming discussion; section 3 presents the data available from the EPICA ice core (microstructure, dust content, ion concentrations, bubbles and clathrates evolution) and an analysis of the localization of dust particles within the ice from X-ray tomography; section 4 describes the motivations for modeling the mean grain size evolution as well as the structure of the proposed model; section 5 discusses the different mechanisms which could explain the grain size profile, on the basis of (1) the correlation between grain size and other parameters and (2) the results of the model. Section 6 presents our conclusions.

2. Grain Growth in Polycrystalline Materials

2.1. Growth Kinetics Without Impurities

[6] The driving force for grain growth in polycrystalline materials is a reduction in the total grain boundary energy within the material. To derive growth kinetics, *Burke and Turnbull* [1952] ignored the environment of a grain, that is, the structural and topological constraints within an assembly of grains, and assumed the boundary is part of a sphere. They obtained the following expression for the grain boundary velocity v:

$$v = \mu \frac{\gamma}{R} \tag{1}$$

where μ is the mobility, γ the grain boundary free energy and R the grain radius. Further assuming that dR/dt is proportional to v, that is $\frac{dR}{dt} = \mu \frac{\alpha\gamma}{R} = \mu P$ (where α is a small geometric constant, and $P = \alpha\gamma/R$ represents the driving force), they deduced the following, so-called parabolic, grain growth kinetics:

$$R^2 - R_0^2 = 2Kt \tag{2}$$

where R_0 is the initial grain size and K is an Arrhenius temperature-dependent constant.

[7] One of the shortcoming of the *Burke and Turnbull* [1952] analysis was to ignore the topological space-filling requirements within an assembly of grains. As a consequence of these requirements, large grains grow at small grains expense. The simplest way to model these requirements is a mean field approach that considers an isolated grain embedded in an environment representing the average effect of the whole array of grains. Such approach was proposed by *Hillert* [1965], and predicted a parabolic growth kinetics. Other mean field theories of grain growth have been proposed in the literature [see, e.g., *Humphreys and Hatherly*, 1996], most of them predicting parabolic growth kinetics as well.

[8] The exponent 2 in equation (2) is a lower bound derived from mean field approximations. Most of the experimental data in different materials are better described by

$$\langle R \rangle^m - \langle R_0 \rangle^m = 2K't \tag{3}$$

with m lying between 2 and 5 [*Higgins*, 1974; *Ralph*, 1990]. $\langle R_0 \rangle$ is the average grain size at time $t = 0$ and K' is the apparent grain growth constant. On the other hand, numerical models of grain growth based on Monte Carlo simulations [*Anderson et al.*, 1989] or on vertex dynamics [*Weygand et al.*, 1998] give values of m very close to the lower bound 2. Therefore departure from $m = 2$ is thought to result from solute drag [*Fan et al.*, 1999], interactions with microparticles, the effect of texture, or a nonsteady state regime [*Ralph*, 1990].

2.2. Grain Size Distributions

[9] In the regime of normal grain growth, the distribution of normalized grain sizes $R_i/\langle R \rangle$ remains unchanged, unimodal, and is generally well fitted by a lognormal distribution [*Humphreys and Hatherly*, 1996; *Ralph*, 1990]. To date, however, this lognormal fit has no theoretical support. In fact, *Hillert* [1965] deduced, from his mean field approach, a unimodal distribution slightly different from a lognormal. If one starts from a distribution with a different shape (at $t = 0$), a transient regime is observed with an evolving distribution [*Weygand*, 1998]. Normal grain growth only refers to the steady state. Whereas solute drag does not modify the shape of the distribution, microparticles do (see below).

2.3. Effect of Impurities

[10] Grain growth can be affected by different kinds of impurities including solutes, insoluble microparticles, or gas bubbles.

2.3.1. Solutes

[11] In a low-velocity/low–driving force regime relevant for polar ice [*Alley et al.*, 1986a], solutes are dragged by the moving boundaries. This drag of impurities reduces the grain boundary mobility μ. The classical model of this effect, developed independently by *Cahn* [1962] and *Lücke and Detert* [1957] is of the form

$$\mu(c) = \frac{\mu_i}{1 + \mu_i \lambda c} \tag{4}$$

where c is the impurity concentration, μ_i the intrinsic mobility of the boundary and λ a constant [see also *Lücke and Stüwe*, 1971]. This classical model does not predict any modification of the exponent m in the grain growth equation. However, recent 2D numerical simulations [*Fan et al.*, 1999] suggest that solute drag may significantly increase m when the solute diffusivity in the lattice is small compared to the intrinsic boundary mobility. In any case, solute drag does not modify the normalized grain size distribution [*Fan et al.*, 1999]. Indeed, a reduction of mobility would apply equally to all grain boundaries. In this situation, although the global kinetics would be slowed down, the behavior of one grain relative to others would remain unchanged, and so would the normalized distribution of grain sizes.

2.3.2. Second-Phase Particles

[12] Large (relatively to solute atoms) second-phase particles, such as dust particles in polar ice, cannot be dragged by a moving boundary. Rather, they pin these boundaries. The role of pinning on the grain growth process depends on the location of particles (see below), as well as on the ratio between the average grain size and the mean distance between particles. For small grain sizes compared to large interparticle distances, most of the boundaries "do not feel" the particles and so the global growth process is unchanged. For small interparticle distances, most of the boundaries are pinned and the growth process is completely stopped. A transient behavior is found in between [*Humphreys and Hatherly*, 1996; *Weygand et al.*, 1998].

[13] Zener (cited by *Smith* [1948]) was the first to model this pinning effect. The interaction between a boundary of free energy γ and a spherical particle of radius r_d leads to the following restraining force F_Z:

$$F_Z = \pi \gamma r_d \tag{5}$$

Averaging the effect of N_d particles per unit volume gives an expression for the (average) pinning pressure P_Z exerted by the particles on unit area of boundary, assuming that all the particles have the same radius r_d [*Humphreys and Hatherly*, 1996]. P_Z depends on the particle distribution within the matter. It is larger when particles are concentrated along the boundaries or at grain vertices rather than distributed randomly within the volume, as the boundaries "feel" a larger particle density. As shown below, this point is essential in the case of polar ice. Corresponding expressions for P_Z are given in Table 1. This pinning pressure works against the driving force for grain boundary motion, P. Hence, in the presence of pinning, equation (1) can be modified as [*Humphreys and Hatherly*, 1996]:

Table 1. Expressions for P_{Z_x} and R_{Z_x}[a]

	Particles Distributed Randomly	Particles Along Grain Boundaries	Particles at Grain Vertices
P_{Z_x}	$2\pi\gamma {r_x}^2 N_x$	$\pi\gamma r_x R N_x/3$	$\pi\gamma r_x R N_x$
R_{Z_x}	$\frac{\alpha}{2\pi r_x^2 N_x}$	$\left(\frac{3\alpha}{\pi r_x N_x}\right)^{\frac{1}{2}}$	$\left(\frac{\alpha}{\pi r_x N_x}\right)^{\frac{1}{2}}$

[a] P_{Z_x} is the pinning pressure exerted by N_x objects (dust particle, bubble, or clathrate), and R_{Z_x} is the induced limiting grain size. The expressions of P_{Z_x} can be added to estimate the total contribution of (1) different objects x or (2) x-type objects with different size r_x. The corresponding limiting radius is deduced from equation (6) with $\frac{dR}{dt} = 0$.

$$\frac{dR}{dt} = \mu(P - P_Z) = K\left(\frac{1}{R} - \frac{1}{R_Z}\right) = K_0 e^{\frac{-E_A}{R_G T}}\left(\frac{1}{R} - \frac{P_Z}{\alpha\gamma}\right) \tag{6}$$

where $K = \mu\alpha\gamma$ is an Arrhenius temperature-dependent constant, with an activation energy E_A and a grain growth constant K_0 expressed in $mm^2\ yr^{-1}$, and R_G is the perfect gas law constant. Equation (6) shows clearly the nonlinear decay of the growth rate dR/dt toward zero as the grain size R approaches R_Z. In the limiting case $P = P_Z$, the growth process is stopped and Zener [*Smith*, 1948] deduced a corresponding limiting (maximum) grain size R_Z whose expressions are given in Table 1. Zener originally set the geometrical constant α to 1, but more recent models and observations argue for lower values between 0.25 and 0.5 [*Humphreys and Hatherly*, 1996]. During the transient stage when R increases toward R_Z, the growth rate dR/dt, driven by $P - P_Z$, decreases toward zero. This may be (incorrectly) interpreted as an (apparent) increase of the exponent m in the growth kinetics (equation (3)) compared to the lower bound $m = 2$.

[14] It is worth noting that unlike the drag of solutes, pinning does not reduce the mobility μ, but rather modifies not uniformly the driving force for boundary migration. Consequently, normalized ($R_i/\langle R\rangle$) grain size distributions are modified by pinning [*Riege et al.*, 1998]. Analytical models [*Abbruzzese and Lucke*, 1992], 2D [*Weygand*, 1998] and 3D [*Song et al.*, 2000] numerical simulations of Zener pinning, and some experimental evidence [*Tweed et al.*, 1982] argue for narrower normalized distributions (i.e., smaller standard deviation) for pinned microstructures, whereas [*Riege et al.*, 1998] reported a shift of the mean for a 2D simulation.

[15] Under some circumstances, GB may unpin from particles or pores. This process has been explored by *Gore et al.* [1989], who showed that a thermally activated unpinning of GB from submicronic particles in ferrous alloys could lead to an underestimation of the grain size by the classical Zener approach. *Gore et al.* [1989] proposed the following expression for the ratio of impurities leaving GB per unit time, that is, the rate of unpinning, dp_U/dt:

$$\frac{dp_U}{dt} = \nu_0 \exp\left(-\frac{E_U}{R_G T}\right) \tag{7}$$

where ν_0 is the attempt frequency for unpinning, R_G the perfect gas law constant and E_U is an activation energy. During dt, the proportion of dust particles randomly distributed p_{ran} increases by dp_U, whereas the proportion of dust particles along grain boundaries p_{gb} decreases by dp_U. As p_{ran} increases to the detriment of p_{gb}, the unpinning process implies an increase of the limiting grain size, therefore allowing further normal grain growth. ν_0, and consequently dp_U strongly decreases with increasing average particle radius. At timescales relevant to metallurgy (~hours), unpinning is significant for particle sizes below 100 nm, that is, much smaller than the dust particles contained within polar ice (~1 μm). However the timescales involved in ice sheet flow are 8 to 10 orders of magnitude larger, making the unpinning likely within polar ice. This problem will be discussed in more details in section 5.7.

2.3.3. Bubbles

[16] The effect of gas bubbles in polar ice on grain growth can be considered as being intermediate between solute drag and particles pinning. Bubbles exert a pinning effect on grain boundaries in a similar manner to second-phase particles [*Alley et al.*, 1986a; *Humphreys and Hatherly*, 1996]. The mechanisms and relations summarized in the previous section are therefore relevant. However, once the average grain size has reached the limiting grain size set by the bubbles, grain boundaries can drag the bubbles in a low-velocity regime, therefore allowing further (slow) grain growth. In this case, the boundaries mobility is dictated by the bubble mobility. This bubble mobility depends on the diffusion mechanism allowing transport of matter across the bubble, which can be either vapor diffusion, surface diffusion, or lattice diffusion [*Nichols*, 1966]. As shown below and already discussed by *Alley et al.* [1986a], in the shallow part of cold ice sheets where bubbles are still present, their associated limiting grain size is much larger than the average grain size, therefore excluding the relevance of this low-velocity regime. Such analysis led [*Alley et al.*, 1986b] to conclude that, for the Byrd ice core, the bubbles slow the grain growth in shallow ice by about 10%.

2.4. Rotation Recrystallization

[17] The effect of the rotation recrystallization on the grain size can be estimated following the dislocation density-based modeling framework proposed by *Montagnat and Duval* [2000]. The evolution of the dislocation density ρ with depth is the result of different terms: (1) the increase of ρ due to the work hardening and (2) a decrease of ρ induced by the grain boundaries migration as dislocations located in the area swept by the boundary disappear. Then, the evolution of the dislocation density can be expressed as

$$\frac{d\rho}{dt} = \frac{\dot{\varepsilon}}{2bR} - \frac{\beta\rho\frac{dR}{dt}}{R} \tag{8}$$

where $\dot{\varepsilon}$ is the strain rate, b the Burgers vector, $\frac{dR}{dt}$ is defined by equation (6) and β is a coefficient which indicates a possible heterogeneous location of the dislocations within the grain (i.e., higher density near grain boundaries if $\beta > 1$).

[18] The decrease of the dislocation density by the formation of a subboundary can be calculated assuming that subgrains misoriented by an angle θ contain only geometrically necessary dislocations. Therefore the associated dislocation density $\rho_{sb} = \frac{\theta}{bR}$ is consumed for the formation of a subboundary of average size $2R$. It is further assumed that when θ reaches a threshold value $\theta_c = 5°$, the subboundary becomes a true grain boundary. Averaged over the whole grain population, this threshold value θ_c corresponds to a threshold dislocation density ρ_c. Rotation recrystallization is assumed to start when ρ reaches ρ_c. If ρ exceed ρ_c, the dislocation density excess $\Delta\rho = \rho - \rho_c$ produced by the deformation (integration of equation (8)) is entirely consumed by the rotation recrystallization. Following this assumption, rotation recrystallization induces a negative contribution to the grain growth rate:

$$\frac{dR}{dt}\Big|_{prg} = -\frac{bR^2}{\theta_c} \times \frac{d\rho_{sb}}{dt} = -\frac{bR^2}{\theta_c} \times \frac{\Delta\rho}{\Delta t} \tag{9}$$

3. Available Records for Microstructure and Impurities

[19] A large part of the present work is based on data recorded along the EPICA ice core at Dome Concordia, Antarctica (75°06′S, 123°20′E, elevation 3233 m a.s.l). This ice-coring program reached the depth of 3270.20 m during the 2004–2005 field season. Here we present an analysis of the microstructure from 100 m (firn-ice transition) to 2200 m. The Dome Concordia ice core provides a unique opportunity for a study of grain growth within cold ice sheets (as well as other recrystallization phenomena), as detailed records of the microstructure, dust content and chemistry are available.

[20] As grain growth is a time-dependent process, the different records analyzed below have been plotted against the depth as well as the age of the layer. We used the official dating model for the depth-age correspondence [*EPICA Community Members*, 2004].

3.1. Microstructure

[21] Vertical thin sections of ice were prepared in the field along the EPICA core between 100 m (which corresponds roughly to the close-off depth) and 2200 m, then digitized and analyzed using an image analysis processing described by *Gay and Weiss* [1999] in order to extract the microstructure in 2D. An example of extracted microstructure is shown in Figure 1. At least, one section has been digitized every 10 m of the core. Around each climatic transition, which are associated with a change in the mean grain size, we increased the sampling rate to one section every 5 m or more. In addition, thin sections were prepared and digitized at depths corresponding to special events such as a dust layer or a dielectric profiling (DEP) peak [*Wolff et al.*, 1999]. Because we used the same image resolution everywhere (1 pixel = 50 μ*m*) and because the mean grain size is generally increasing with depth, we adjusted the image size individually between 30 × 20 mm^2 and 40 × 60 mm^2 in order to always sample a statistically significant grain population, that is, more than 100 grains.

[22] The average grain size (or grain radius) $\langle R \rangle$ was calculated over the entire population of grains of a section by the arithmetic average of the square root of the grain

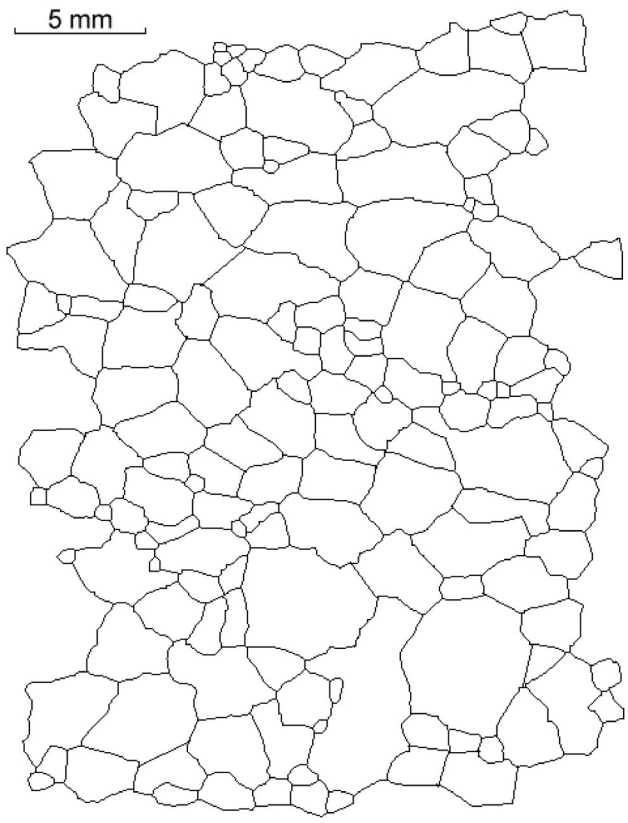

Figure 1. Example of a microstructure extracted from image analysis at a depth of 709 m. The vertical axis of the image corresponds to the true in situ vertical axis of the core.

area, $\langle A^{\frac{1}{2}} \rangle$. This definition differs from the methods previously used to determine manually the average grain size on thin sections of polar ice, such as the linear intercept method [*Alley and Woods*, 1996] or the average size of the 50 largest grains within the section [*Gow*, 1969]. However, as stressed by *Gay and Weiss* [1999], the estimation of $\langle R \rangle$ from $\langle A^{\frac{1}{2}} \rangle$ gives the best 2D estimate of 3D grain growth kinetics.

[23] The standard deviation on the estimation of the average grain size, $\sigma_{\langle R \rangle}$, has been estimated from a 3D numerical Potts model, known to well reproduce the topology of a 3D microstructure under normal grain growth [*Anderson et al.*, 1989]. On this modeled 3D microstructure we estimated the standard deviation of $\langle R \rangle$ induced by calculating $\langle R \rangle$ from a 2D cut of a 3D microstructure, as well as the standard deviation induced by the number of grains, N_g, within the section: $\sigma_{\langle R \rangle}/\langle R \rangle = 0.02 + 0.44 \times N_g^{-1/2}$ [*Durand*, 2004].

[24] All the observed distributions of normalized grain sizes are well fitted by lognormal distributions (see *Arnaud et al.* [2000] for examples within the shallow part of the ice sheet). These distributions are therefore characterized by only two independent parameters, the average and the standard deviation of $\ln (R_i/\langle R \rangle)$.

[25] Figure 2 shows the profiles of the average grain size $\langle R \rangle$ (Figure 2a), of the two parameters of the distributions (Figures 2b and 2c), along with the available deuterium profile [*EPICA Community Members*, 2004] which is a proxy of local temperature change (Figure 2d). Figure 2 shows an increase of the average grain size with time, however punctuated by abrupt decreases clearly synchronous with Termination I, with the transition between stages 3.3 and 4.2, and with termination II. Interestingly, the two parameters of the normalized distribution show also synchronous variations with deuterium, despite a larger signal/noise ratio. The fact that $\langle R \rangle$ still increases with depth down to 2200 m indicates that rotation recrystallization is unable to fully balance grain growth, as it was observed for the Vostok core.

[26] The Holocene is characterized by a very stable climatic signal as well as low-soluble and insoluble impurity contents (except for specific layers associated with volcanic events). Nevertheless, the Dome Concordia grain size data within the Holocene (100–450 m) departs from equation (2), as it is best fitted by equation (3) with $m = 3.2 \pm 0.2$, $K' = 2.8 \times 10^{-4} \pm 0.2 \times 10^{-4}$ and $\langle R_0 \rangle = 3.10^{-5} \pm 1.10^{-5}$ mm. A similar observation was reported by *Thorsteinsson et al.* [1997] for the GRIP ice core with $m = 2.5$, though not explained. As discussed in section 5.4, this departure from the theoretical parabolic growth law (equation (2)) is likely the result of bubbles pinning. Note that the physical meaning of the value of $\langle R_0 \rangle$ has to be taken with caution, as it does not correspond to a measured value of grain size at the ice sheet surface: different processes other than normal grain growth could take place within the snow and the upper firn.

[27] In some places, "continuous" grain size analyses have been performed. Vertical thin sections of 55 or 110 cm long have been digitized to extract the microstructure. Then, linear intercept analysis was performed along horizontal lines at a resolution of 1 pixel, that is, 50 μm. The relation between the average linear intercept $\langle L \rangle$ and the average grain size $\langle R \rangle = \langle A^{\frac{1}{2}} \rangle$ depends on the morphology of the grains [*Underwood*, 1970]. In the present case, the ratio $\langle L \rangle / \langle R \rangle$ was found stable around 1.15 [*Gay and Weiss*, 1999]. The linear intercept measurements of the continuous analyses have been corrected consequently. These continuous analyses allowed to study special events such as volcanic eruptions (see section 5.5).

3.2. Impurities

[28] Section 2 has stressed the importance of impurities for grain growth in polycrystalline materials. Impurities contained in polar ice can be classified in two categories: insoluble and soluble (in water after melting).

3.2.1. Insoluble Second-Phase Particles

[29] In polar ice, insoluble impurities consist of dust microparticles that are of two different origins: continental aerosols and volcanic ashes. The number and size distribution of dust particles has been measured along the Dome Concordia ice core down to 2200 m with a sampling period of 5.5 m using a Coulter counter. The record is detailed and analyzed by *Delmonte et al.* [2002, 2004]. The number of particles N_d per unit volume of ice, shown in Figure 2e, exhibit very strong variations synchronous with climate changes, as observed previously in other ice cores [*Petit et al.*, 1999; *Steffensen*, 1997]. The particle radius distributions are well fitted by lognormal distributions. To estimate the pinning pressure resulting from the particles, P_Z, we

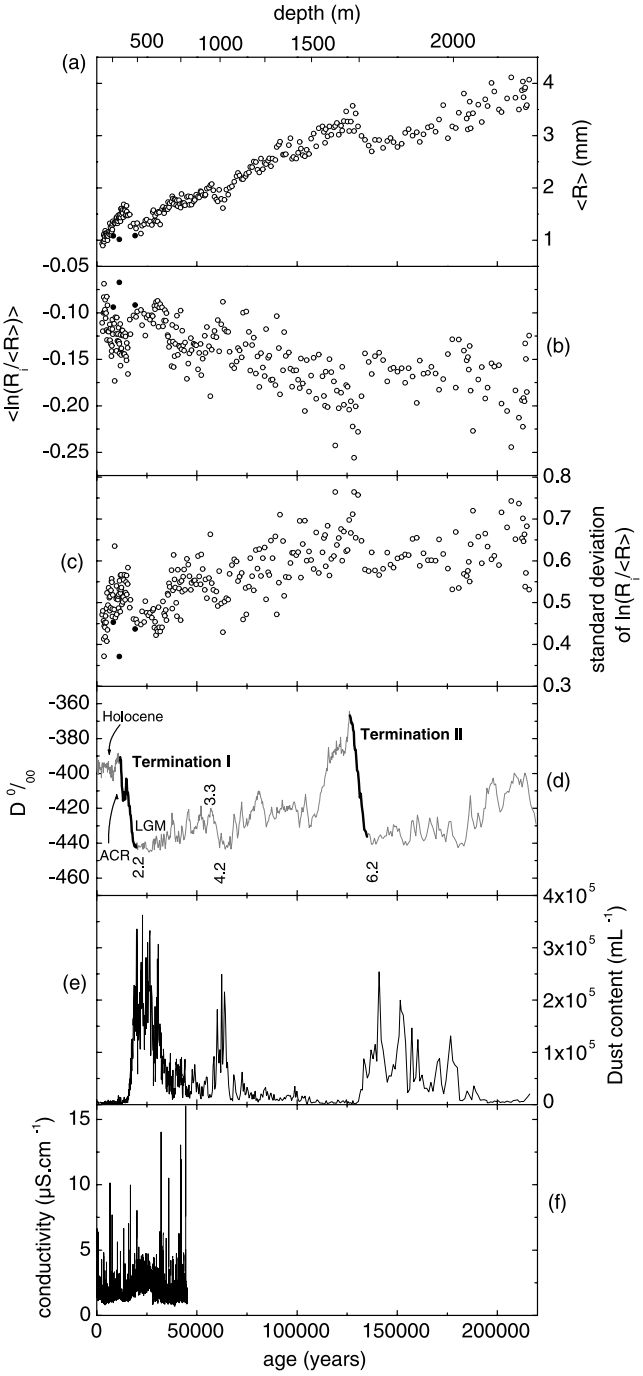

Figure 2. (a) Average grain size profile of the EPICA ice core at Dome Concordia. The circles correspond to volcanic ash layers. (b) Normalized grain size distributions: evolution of $\langle \ln(R_i/\langle R \rangle) \rangle$. (c) Normalized grain size distributions: evolution of the standard deviation of ln $(R_i/\langle R \rangle)$. (d) Deuterium profile [from *EPICA Community Members*, 2004]. Principal climatic stages are pointed out, and terminations I and II are highlighted by the thick black lines. (e) Dust content (number of particles) [from *Delmonte et al.*, 2004]. (f) Liquid conductivity measured by CFA. The corresponding depth-age relationship is given by EDC2 dating [*EPICA Community Members*, 2004].

summed the contributions of all the classes of size of the distribution, from the notation of Table 1. Note also that the mode of the distribution is also slightly changing with climate, for example, from 1.03 ± 0.10 mm in Holocene to 0.96 ± 0.01 mm for LGM (for the volume-size distribution) [*Delmonte et al.*, 2002]. However, in terms of pinning effect (section 2.3.2 and Table 1), this 7% increase of the mode from LGM to Holocene is completely negligible compared to the decrease of the number of particles by a factor of about 50.

3.2.2. Localization of Dust Particles

[30] As explained in section 2.3.2, the average pinning effect of particles on grain growth depends on how the particles are distributed within the matter. Assuming a uniform distribution of particles within the volume, *Alley et al.* [1986b] concluded that the amounts of dust measured in polar ice were not large enough to significantly affect grain growth, except for layers with volcanic ashes. However, scanning electron microscopy observations of surfaces of Dome Concordia ice samples suggest that a large proportion of particles are located along GB [*Barnes et al.*, 2002]. This may not be the case for Greenland (GRIP) ice [*Barnes et al.*, 2002].

[31] An EPICA ice sample taken at a depth of 578.05 m corresponding to LGM ice was analyzed using X-ray tomography [*Peix et al.*, 2000] at the European Synchrotron Research Facility in Grenoble (ESRF). This non destructive technique gives series of superposed 2D images that are used to build a 3D image of the analyzed volume. The resolution (the voxel size) was 0.923 μm^3. The analyzed volume was a cylinder with a diameter of 1024 pixels and a height of 3072 pixels. Because of the limited sampled ice volume (1970 mm^3), only few grains and GB were contained in this sample. Dust particles of the order of, or larger than the voxel size were easily identified and located, therefore giving a 3D spatial distribution of dust particles (Figure 3). Given the resolution of the analysis, only the largest particles were located, as the mean diameter of particles is around 1 µm. Coupled with the fact that GB are not resolved by this tomography, it implies that a clear structure is difficult to discern in Figure 3. Instead, we performed a correlation analysis of the particle locations in order to determine the correlation dimension [see, e.g., *Korvin*, 1992]:

$$C(x) = \frac{2}{n(n-1)} N_{ca}(x' < x) \tag{10}$$

where n is the number of locations considered and N_{ca} $(x' < x)$ the number of pairs of locations separated by a distance x' smaller than x. The scaling of $C(x)$ gives the dimension D of the support of the distribution, $C(x) \sim x^D$. For the dust particles, we found $D = 1.45 \pm 0.1$ (thick line in Figure 4). To test the confidence level on this measure as well as a possible effect of the geometry of the sample, we simulated three types of random spatial distributions of particles within the sampled volume. The first (second) type of distribution corresponds to particles randomly distributed along a line (along a plane) contained in the cylinder. For the third type, the particles were randomly distributed within the volume (Poisson distribution). The correlation analysis of these distributions is shown in Figure 4. The

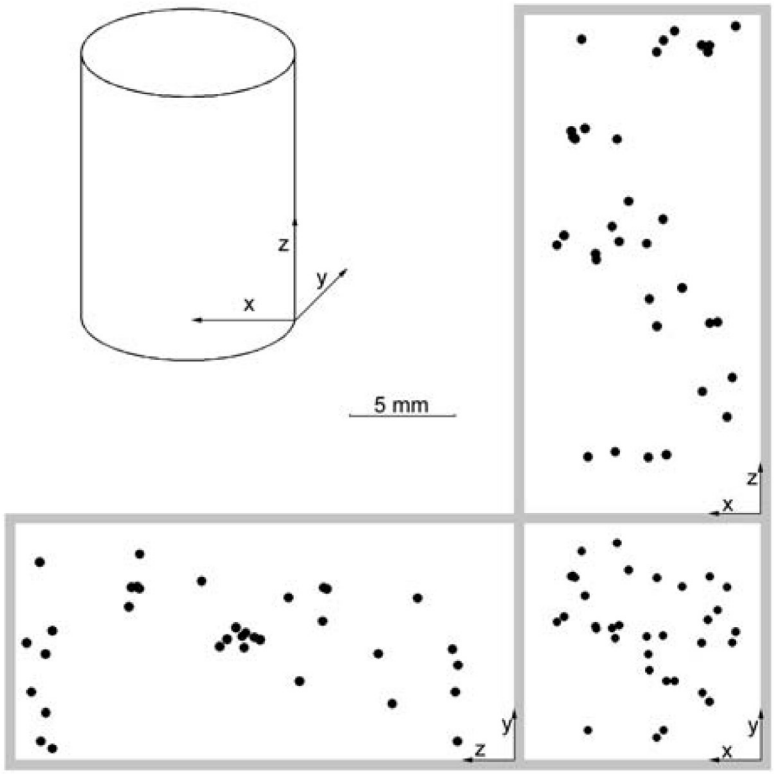

Figure 3. Three-dimensional localization of microparticles measured from an X-ray tomography of an ice sample taken at a depth of 578.05 m. The volume analyzed was a cylinder with a diameter of 1024 pixels and a height of 3072 pixels. One pixel corresponds to 0.92 μm. The projections of the particle locations on three perpendicular planes are shown.

experimental data are comparable with the planar random distributions, but cannot result from a 3D random distribution. This indicates that the particles (at least the largest ones) are not uniformly distributed within the volume, rather over a surface. GB being the only 2D structures within polar ice at this depth, this analysis strongly suggests that dust particles are located along GB. Moreover, as the correlation dimension is significantly lower than 2, this analysis suggests a possible clustering (near grain edges?) of particles over the GB.

3.2.3. Soluble Impurities

[32] The soluble impurity content of the Dome Concordia ice core is known from continuous flow analysis (CFA) [*Röthlisberger et al.*, 2000] and fast ion chromatography (FIC) [*Traversi et al.*, 2002]. CFA gives a complete record of the liquid conductivity, as well as of major ions (Na^+, Ca^{2+}, NO_3^-, NH_4^+), at a resolution of approximately 1 cm, while FIC measurements of Cl^-, NO_3^- and SO_4^{2-} resulted in a resolution of approximately 4 cm. Liquid conductivity (Figure 2f) has been considered as a proxy of the total soluble impurity content [*Hammer*, 1977; *Fisher and Koerner*, 1986]. However, this relation between liquid conductivity and soluble impurity content is complex, different species contributing differently to the total conductivity.

[33] CFA does not provide information about the localization of these impurities (within the lattice, within inclusions, along grain boundaries), or about their nature

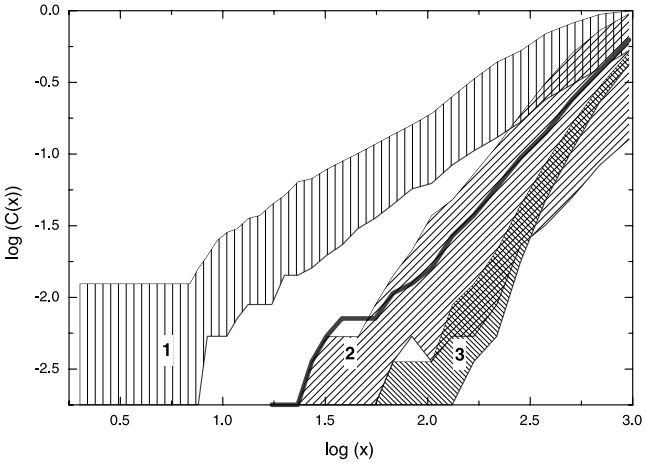

Figure 4. Correlation analysis of the spatial distribution of particles. The thick line represents the correlation analysis of the data plotted in Figure 3. Hatched zone 1 represents correlation analyses for distributions of particles randomly distributed along a line contained within the sampled cylinder. This zone shows the variability of this analysis for various random distributions along various lines. Hatched zone 2 is the same as hatched zone 1 but for particles randomly distributed over a plane. Hatched zone 3 is the same as hatched zone 1 but for particles randomly distributed within the cylinder.

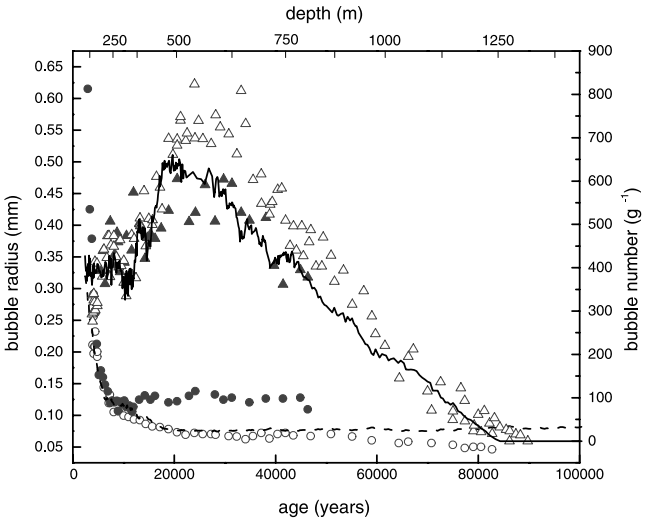

Figure 5. Evolution of the average bubble radius (circles) and of the bubble density (triangles) with depth. Open symbols represent the Vostok ice core [*Lipenkov*, 2000], and solid symbols represent the EPICA Dome Concordia ice core (this work). Solid lines show bubble density, and dashed lines show the radius estimated by the model. Note that the top axis corresponds to Dome C depths.

(solutes, precipitates, aqueous solutions along boundaries). Whereas X-ray microanalysis has shown that H_2SO_4 is concentrated along grain boundaries and especially at vertices, sea salts (essentially NaCl) do not show such localization [*Fukazawa et al.*, 1998; *Wolff et al.*, 1988]. Recent chemical analyses of large single crystals in the bottom of the Vostok ice core [*Montagnat et al.*, 2001] show large and spatially homogeneous concentrations (up to 1 ppm) of salts (Na and Cl) that argue for the presence of these species as solutes. In both cases, it is fair to assume that the effect of these soluble impurities on grain growth, if any, will be through a decrease of GB mobility (section 2.3.1), although the quantification of this effect (e.g., the parameter λ in equation (4)) is completely unknown.

3.3. Bubbles and Clathrates

[34] In polar ice, bubbles result from the closure of porosities during densification. Therefore they are, at least initially, located at grains vertices or along GB. Then, their size decreases as they are closing with depth. When the overburden pressure is large enough, clathrates form. Clathrates pin the boundaries, as dust particles and bubbles do [*Uchida et al.*, 1993], although the evolution of clathrates with depth and time, as well as their interaction with GB, are still unclear.

[35] The information available on the bubble content of the Dome Concordia ice core is limited to the first 800 m (Figure 5). Consequently, we completed this data set with the more detailed profile measured on the Vostok ice core. Such comparison seems to be relevant as the surface temperature and the accumulation rates of the two sites are relatively similar. However, the measurements of bubbles below 360 m on the Dome C core have been done on relaxed ice. Therefore the measured bubble radius is certainly overestimated compare to their previous radius in unrelaxed state, and the Vostok record (measurement made on fresh ice) gives a better in situ estimation. Considering the location of bubbles, *Gow* [1968] reported a uniform distribution of bubbles whatever the depth along the Byrd ice core. The situation appears to be different for colder ice. Figure 6 shows the relative locations of bubbles and clathrates along the Vostok ice core. These observations show that (1) the bubbles have a preponderant location along GB in shallow ice, and (2) the proportion of bubbles randomly located in the ice increase with depth. This indicates that grain boundaries can partly unpin from bubbles (the same behavior is observed for clathrates).

4. Average Grain Size Evolution: A Model

[36] As mentioned above, most polar ice microstructure studies performed so far focused on correlations between grain size and different parameters. However, because many parameters exhibit variations in phase with the climatic transitions, the correlation studies do not allow selection of one mechanism over another. Moreover, such studies are qualitative in the sense that they cannot provide any information on the relative contribution of the different mechanisms. In order to avoid these problems, we decided

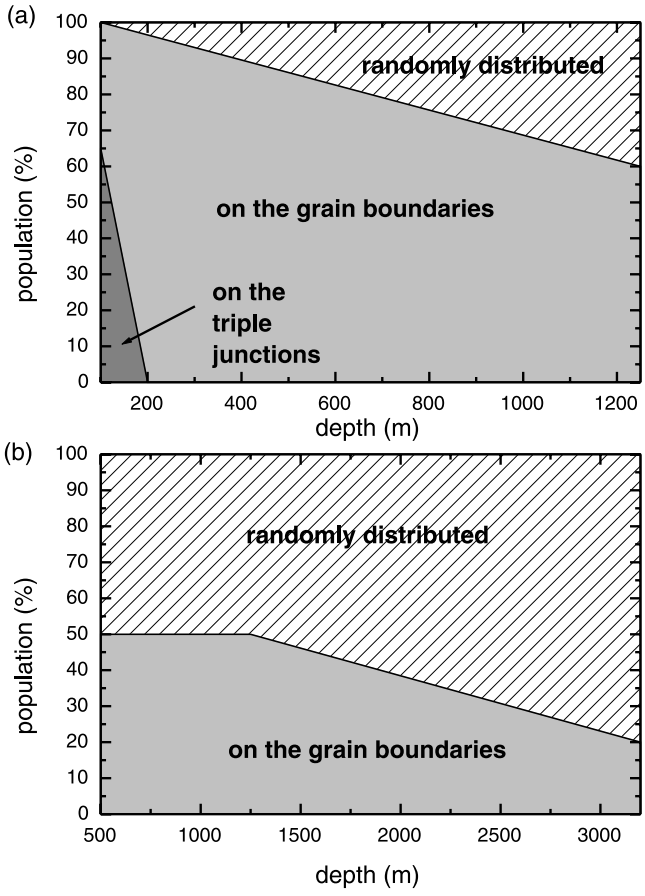

Figure 6. Evolution of the localization of (a) bubbles and (b) clathrates with depth estimated from observations on the Vostok ice core. Note the different depth intervals shown in Figure 6a and Figure 6b, as clathrates form from about 500 m.

to model the grain size evolution along the Dome Concordia core using the equations widely used in material science and summarized in section 2. This enlightens the predominant processes acting against grain growth. Moreover, discrepancies between data and model results might reveal that some mechanism is not taken into account.

[37] The model proposed here is one-dimensional, as it calculates the evolution of the grain size, R, with the vertical coordinate z (the depth) only. It simulates the evolution of an (average) grain size with depth, but does not give any information about grain size distributions. At each time step, the model calculates the grain size increment dR/dt for an ice layer, following equation (6). The integration is performed all along the sinking history of the considered layer, from its deposition to its present depth. Then, the calculation is repeated for many different layers, the ones for which a measure of the dust content is available.

[38] The different processes taken into account in the present model are listed below. The details concerning the implementation of each process into the model can be found by *Durand* [2004, section 3.3].

[39] 1. The normal grain growth is taken into account through the *Burke and Turnbull* [1952] analysis and equation (6).

[40] 2. The temperature changes experienced by the ice layer along its sink are given by a temperature model [*Ritz*, 1989] and affect the normal grain growth rate through the Arrhenius temperature-dependent parameter K. This temperature model takes into account (1) temperature gradients between the surface and the bedrock and (2) the evolution of the surface temperature with climate. These temperature profiles are used as input data for our grain growth model, and cannot be "adjusted" to improve the modeling of the grain size profile.

[41] 3. The pinning effect is also described by equation (6), through the pinning pressure P_Z. It is worth noting that P_Z results from the contribution of different pinning objects: (1) dust particles and (2) bubbles and clathrates. The number and size of dust particles are given by Coulter Counter measurements [*Delmonte et al.*, 2002], and as suggested by our X-ray tomography analysis we first assume that all the particles are located along the grain boundaries (see section 3.2.2). This allows to calculate P_Z induced by the dust particles from the equations given in Table 1. For bubbles and clathrates, the parameters needed to calculate the associated pinning pressure are parameterized from our observations. The bubbles density N_b is estimated through an empirical linear relationship between the number of bubbles and the temperature at the time of deposition (data not shown). Once N_b is known, it allows to estimate the mean bubble radius through the volume of air inclusion V_i, where V_i is estimated through porosity measurements. These rough parameterizations give results in good agreement with the measurements (see Figure 5). In the transition zone, N_b decrease linearly to the benefit of the clathrate density: we assume than one bubble transforms into one clathrate, in agreement with observations [*Lipenkov*, 2000]. Concerning the bubbles and clathrates location, the model simply follows the evolution deduced from our observations (see Figure 6). More Details on the bubbles-clathrates parameterization can be found in work by *Durand* [2004].

[42] 4. Unpinning of grain boundaries from dust particles will also be envisaged using the work of *Gore et al.* [1989] through equation (7). This leads to a change in location of the dust particles, and then induces a decrease of their pinning pressure.

[43] 5. As previously mentioned, rotation recrystallization is likely in the depth range studied here. Its implementation within the model is done through the equations detailed in section 2.4. It is worth noting that this rotation recrystallization module does not introduce any additional adjustable parameter to the model. The values of $\beta = 2$ and $\theta_c = 5°$, used in this work, are based on the work of *Montagnat and Duval* [2000] on the GRIP ice core.

[44] As detailed in the following sections 5.1 and 5.2, several arguments indicate that the memory effect of the surface temperature as well as the drag of soluble impurities do not have a significant impact on the grain size along the Dome Concordia ice core. Consequently, the model does not take these mechanisms into account.

[45] Some of the parameters entering equation (6) have been measured along the Dome Concordia ice core or have been determined from simple physics as well as empirical relations (see *Durand* [2004] for details). The three remaining key parameters, K_0, E_A and α, cannot be estimated directly from independent measures along the core. To set the values of the triplets (K_0, E_A, α), we calculated the mean deviation between the model and the data over the depth range 100–500 m, which includes the termination I and the Holocene, for numerous triplets within the ranges $0.25 \leq \alpha \leq 1$, 1.10^7 mm^2.yr$^{-1} \leq K_0 \leq 5.10^8$ mm^2.yr^{-1} and 42 kJ.mol$^{-1} \leq E_A \leq 53$ kJ.mol^{-1}, which are compatible with values given in the literature [*Paterson*, 1994; *Duval*, 1985; *Gow*, 1969]. Note that the values of K_0 and E_A found in the literature are estimated directly from the measurements of the empirical parameter K', therefore the effects of impurities on normal grain growth was implicitly taken into account.

[46] In a first step, we eliminated the triplets which deviate from the data more than the intrinsic variability of $\langle R \rangle$ (see section 3.1). This constrains α within the range 0.25–0.5, and the couple (K_0, E_A) within a band of values that correspond to the same value of the growth rate $K = K_0 \exp(-E_A/RT) = 1 \times 10^{-4}$ mm^2.yr^{-1}. Indeed, as the upper ice sheet is almost isothermal, the sensitivity of K to the temperature is small within the depth range 100–500 m. We fixed the activation energy to 46 kJ.mol^{-1}, close to the median value of the acceptable range. Consequently, K_0 is fixed to 1.10^7 mm^2.yr^{-1}. The sensitivity of the model on α is larger, and the best fit between R and $\langle R \rangle$ within the depth range 100–500 m is obtain for $\alpha = 0.25$. This low value of α expresses a strong effect of pinning (equation (6)). With the triplet (K_0, E_A, α) fixed, we can now model the whole grain size profile down to 2135 m, and test its sensitivity to different parameters such as the temperature, the bubble or the dust content.

5. Critical Review of the Possible Mechanisms That Could Explain the Grain Size–Climate Correlations

[47] As indicated in the introduction, several explanations have been proposed and debated in the literature to explain

the observed synchronous evolution of grain size and climate. They will be reviewed below in the light of the data described in section 3 and the results of the model (see section 4).

5.1. Memory Effect of the Surface Temperature Conditions at the Time of Deposition

[48] *Petit et al.* [1987] proposed that the growth rate K could depend on the temperature of the snow at the time of deposition. They assumed that the grain boundary mobility μ, and consequently K, were proportional to the concentration of interstitials (point defects), c_i, which in turn was supposed to follow an Arrhenius temperature dependence: $c_i \sim \exp(-E_f/RT_0)$, where E_f is an apparent formation energy of interstitials and T_0 is the surface temperature at the time of deposition. In terms of grain boundary velocity, the interstitials are assumed to affect the mobility μ, but not the driving force. With this mechanism, the average grain size becomes a true paleothermometer. The mechanism was proposed on the basis of a good correlation between the $\delta^{18}O$ record and the average grain size for the former Dome C ice core [*Duval and Lorius*, 1980]. This mechanism was questioned by *Alley et al.* [1988] who argued that the diffusion of the interstitials within ice would destroy the memory effect proposed by *Petit et al.* [1987]. See also the reply [*Petit et al.*, 1988].

[49] Besides the objection of *Alley et al.* [1988], the scenario proposed by *Petit et al.* [1987] seems in contradiction with different observations listed below.

[50] 1. The Antarctic Cold Reversal (ACR), clearly identified on the δD record between 12,000 and 15,000 BP (Figure 2d) [*Jouzel et al.*, 2001], is not marked by any grain size decrease on the present profile (Figure 2a), in contradiction with a direct effect of surface temperature. Note that we increased the sampling rate during this period to properly check this point. In the reverse, the transition from stage 3.3 to stage 4.2 around 58,000 BP is marked by a grain size decrease as large as the decreases observed for termination I and II whereas the corresponding surface temperature drop is limited (Figure 2).

[51] 2. As explained in section 2.3.1 for solute drag, a reduction of mobility does not modify normalized grain size distributions. Therefore the profiles of the average and the standard deviation of $\ln(R_i/\langle R\rangle)$ (Figures 2b and 2c) contradict this scenario.

[52] 3. In the shallow ice of Dome Concordia, we identified a few layers with abnormally small grain sizes (marked with solid circles in Figure 2) generally associated with volcanic ash layers detectable by eye (e.g., at a depth of 339.5 m, that is, about 11200 BP). These layers show the same trend as glacial ice for the three independent grain size parameters (Figures 2a, 2b, and 2c). Since there is no reason to expect a high concentration of interstitials associated with these volcanic ash layers in the Holocene, the scenario of *Petit et al.* [1987] is unable to provide a universal explanation for the modification of the ice microstructure.

5.2. Drag of Soluble Impurities

[53] On the basis of correlations between soluble impurity content and grain size along the GISP2 ice core in Greenland, *Alley and Woods* [1996] suggested that soluble impurity drag may significantly affect the grain growth rate, although they acknowledged the noisy character of the data. However, as noted previously, such correlations are not discriminant, as many parameters, including isotopes, conductivity, concentrations of different soluble impurities or of microparticles, grain size, which exhibit simultaneous changes at climatic transitions. Moreover, this hypothesis is in contradiction with the following observations:

[54] 1. Soluble impurities, like interstitials in the scenario of *Petit et al.* [1987] (see above), modify the mobility and not the driving force. Therefore the second argument of section 5.1 holds. That is, soluble impurity drag cannot explain the modification of the normalized grain size distributions.

[55] 2. To analyze possible positive correlations between retardation of grain growth and the soluble impurity content, we define a new adimensional parameter R^*:

$$R^* = \left(\frac{R^2 - R_0^2}{\langle R\rangle^2 - R_0^2}\right) - 1 \tag{11}$$

Here for a given depth corresponding to a measured grain size $\langle R\rangle$, R is the theoretical grain size that the microstructure should have reached at the same depth, assuming a normal grain growth without any impurity effect: it is calculated from the model described in section 4, taking into account only the effect of temperature changes. Combining equations (1), (2) and (4), it can be shown that R^* should be proportional to the impurity concentration c if the grain size profile is explained by soluble impurity drag. Figure 7a shows the relation between the liquid conductivity, taken as a measure of overall soluble impurity content, and R^*. From the chemical records of the Dome Concordia ice core, similar correlations between grain size and different species can be derived, such as SO_4^{2-} (Figure 7b), Na^+ (Figure 7c), or Ca^{2+} (Figure 7d). Once again, as many parameters are changing simultaneously, the correlations observed in some of these figures are not really informative and are associated with a large scatter. Some special layers are more instructive in this respect. These layers, selected in the field from the DEP profile [*Wolff et al.*, 1999] show very large conductivities but "normal" grain sizes ($R^* \approx 0$). This shows that large soluble impurity content do not necessarily imply abnormally small grain sizes, therefore raising questions about the effectiveness of soluble impurity drag to reduce the average grain size. In addition, large R^* values are sometimes associated with relatively low impurity contents.

[56] These observations show that soluble impurities, incorporated into the ice either along GB or as solutes, do not significantly affect the grain growth process. One cannot however exclude a limited effect for very large soluble impurity concentrations and/or physical conditions (e.g., temperature) different from central Antarctica (e.g., in Greenland).

5.3. Variation of K With Temperature

[57] Because K (in equation (6)) is an Arrhenius temperature-dependent constant, colder ice would theoretically imply a smaller growth rate and therefore smaller grains. The activation energy of grain growth in ice is estimated to be within the range 42.4–52 kJ/mol [*Gow*, 1969; *Jacka and*

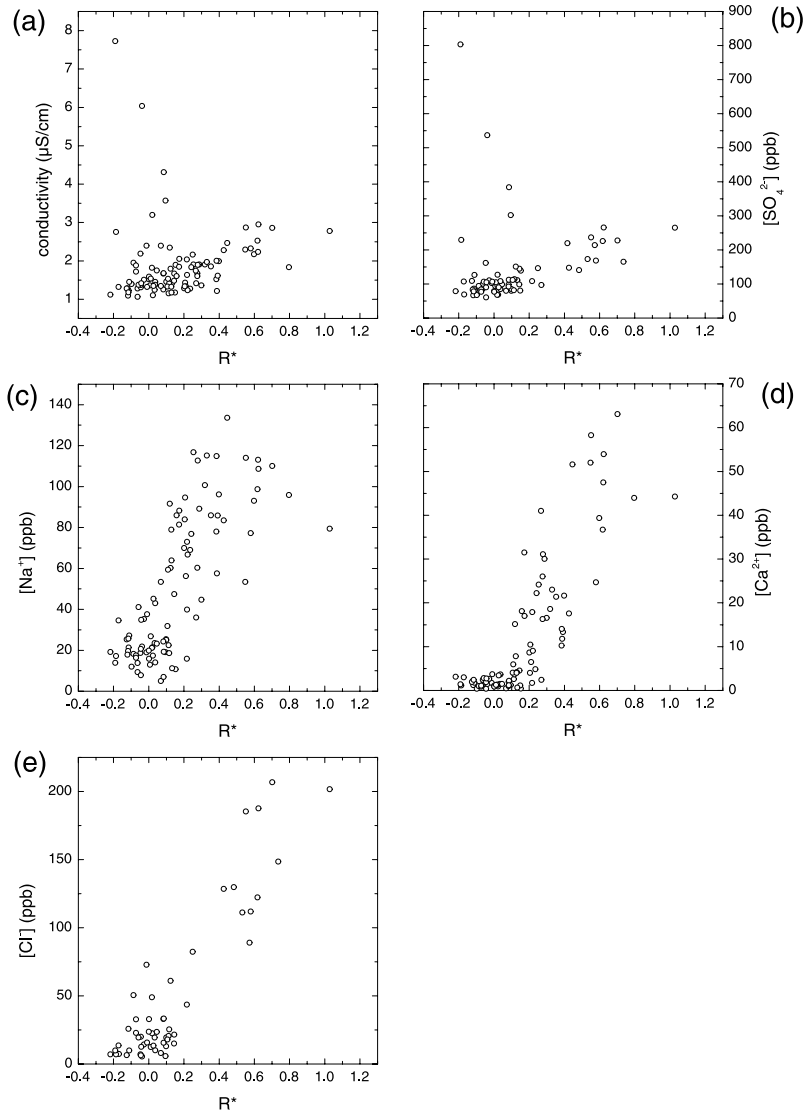

Figure 7. Relationship between the adimensional parameter R^* (see text for details) and soluble impurities over the depth interval 110–786 m for conductivity, $Ca^{2+}$and Na^+, and the interval 110–581 m for Cl^- and SO_4^{2-}: (a) liquid conductivity, (b) SO_4^{2-} concentration [*Traversi et al.*, 2002], (c) Na^+concentration [*Röthlisberger et al.*, 2002], (d) Ca^{2+}concentration [*Röthlisberger et al.*, 2002], and (e) Cl^- concentration [*Traversi et al.*, 2002].

Jun, 1994]. However, as noted by *Duval and Lorius* [1980], the difference in the growth temperature needed to explain the difference in average grain size between Holocene and LGM is far too large compared to surface temperature differences between glacial and interglacial periods. This is confirmed by the model outputs. In a first step, we run the model taking into account only the effect of temperature. It is clear from Figure 8 that the correlation of the grain size profile with climatic transitions is not directly induced by the surface temperature variations. Actually, the strongest effect of temperature is related to the increase of T with z. This is illustrated in Figure 8 by a comparison between an isothermal profile (T = const = −55°C, the current surface temperature) and the profile taking into account all the temperature effects.

[58] In addition, we note that the grain size decrease observed at climatic transitions cannot be explained by a decrease of the initial grain size $\langle R_0 \rangle$ with surface temperature. Indeed, $\langle R_0 \rangle$ deduced from an extrapolation of grain growth to $t = 0$ (see section 3.1) is very small compared to the grain size decrease associated with climatic transitions (e.g., about 0.45 mm for the LGM-Holocene transition).

5.4. Bubbles and Clathrates

[59] As detailed in section 3.1, we observed a grain growth law exponent (m = 3.2) larger than the theoretical exponent (m = 2) during the Holocene. The results of our model strongly suggest that the pinning effect of bubbles is responsible for this increase of m. Figure 9 shows the experimental data and two simulated profiles over the depth range 100–400 m corresponding to Holocene. The first profile takes into account only the temperature effect. It significantly deviates from the data and equation (3) with m = 1.8 is the best fit. In this case m is lower than 2, as the

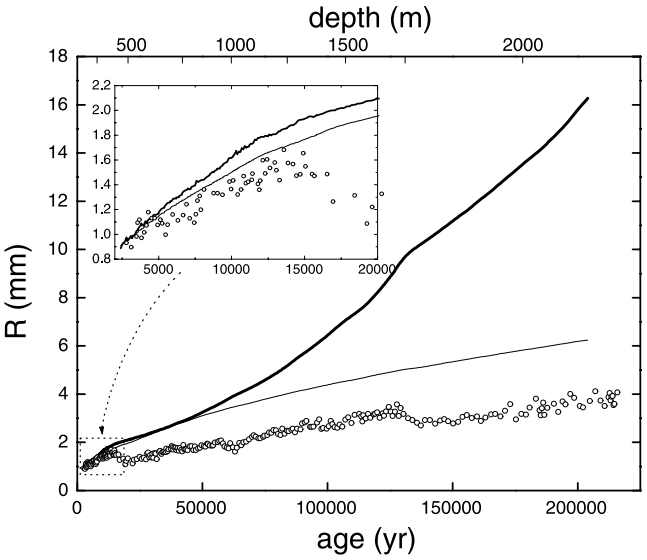

Figure 8. Effect of temperature. Open circles represent the measurements ($\langle R \rangle$), the thick line represents the simulation taking into account only the temperature changes (with age and depth), and the thin line is the simulation for an isothermal ice sheet at −55°C. The inset details the results for the first 20 kyr.

result of the increase of temperature with depth. The second profile takes into account the pinning effect of bubbles and dust (note that the effect of dust is relatively small for this depth range, ∼10%, see later). This simulated profile gives m = 2.7, that is, significantly larger than the parabolic exponent. This shows that the departure of the grain growth law from the theoretical kinetics is most likely the result of bubbles pinning. It is worth noting that R is much smaller than R_Z during the Holocene (see Figure 9a), implying that the boundaries mobility is not governed by the bubbles mobility, as already discussed by *Alley et al.* [1986a].

[60] These effects of temperature increase with depth and of bubbles pinning, which act in an opposite way, are also present in other ice cores. This raises the difficulty of estimating a grain growth rate and a corresponding activation energy from grain size data in shallow ice, assuming a parabolic grain growth law.

[61] In Figure 10 we compare the data to different simulated profiles down to 2135 m. Note that all these simulations include the effects of temperature changes. Not surprisingly, the effect of bubbles and clathrates pinning shown in Figure 10a cannot explain the strong decreases of $\langle R \rangle$ with climatic transitions. However, as R approaches R_Z within deep ice (Figure 9a), clathrate pinning results in a limited grain size decrease observed at termination II. The simulated profiles shown in Figure 10 have been obtained with a low-mobility hypothesis for the clathrates. The extreme opposite situation (i.e., very high clathrate mobility)

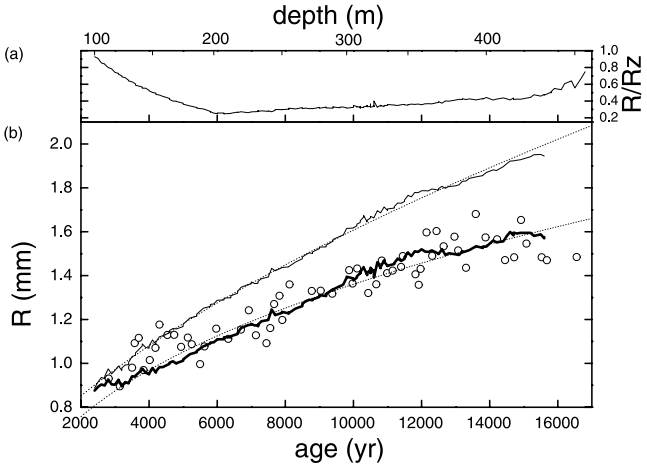

Figure 9. (a) Evolution of the ratio R/R_Z when pinning effects are taken into account during the Holocene. (b) Influence of the pinning effect on the grain growth law exponent during the Holocene. Open circles represent $\langle R \rangle$, and the thin line shows the result when only the temperature effects are taken into account in this simulation. The corresponding dotted line shows the best fit for this simulation, giving m = 1.8. The thick line shows the introduction of the pinning effect of bubbles and dust particles. The corresponding dotted line shows the best fit for this simulation, giving m = 2.7.

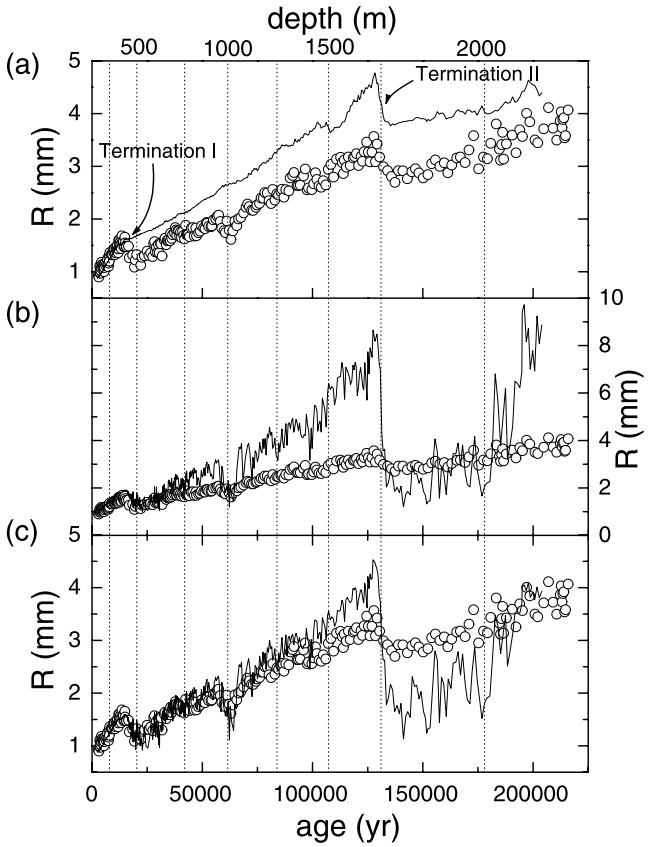

Figure 10. Pinning effect on the grain size evolution. Open circles show measured grain size $\langle R \rangle$. (a) Simulation taking into account the pinning effect of bubbles and clathrates (solid line). Terminations I and II are indicated by the arrows. (b) Simulation taking into account the pinning effect of dust particles (solid line). (c) Simulation taking into account the pinning effect of bubbles, clathrates, and dust particles (solid line).

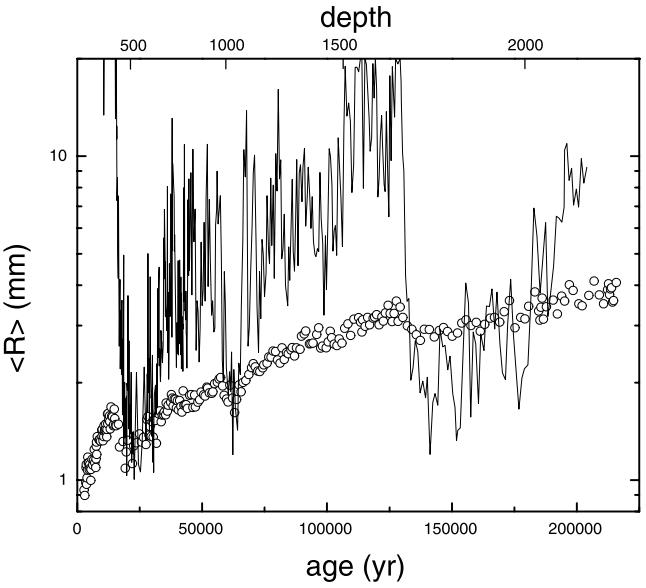

Figure 11. Evolutions of the average grain size $\langle R \rangle$ (circles) and of the limiting grain size R_{Z_d} (thin line) estimated from the dust content and particles located along GB with $\alpha = 0.25$. Note the log scale for the vertical axis.

is unlikely, as it would result into a very large overestimation of the grain sizes below 1200 m (not shown).

5.5. Pinning of Grain Boundaries by Microparticles

[62] As discussed in section 2.3.2 the pinning effect of microparticles on GB can be quantified from the number N_d of particles per unit volume and their distribution of size which are known from Coulter counter measurements (section 3.2.1). Following the discussion of section 3.2.2, we first consider that all the particles are located along GB (possible unpinning of GB from particles is neglected at this stage). Consequently, the limiting grain size associated with the dust particles, R_{Z_d}, is expressed as

$$R_{Z_d} = \left(\frac{3\alpha}{\pi \langle r_d \rangle N_d} \right)^{\frac{1}{2}} \tag{12}$$

where $\langle r_d \rangle$ is the average size of dust particles. In Figure 11, the evolution of R_{Z_d} deduced from the dust record with $\alpha = 0.25$ is plotted. Note that we were unable to calculate R_{Z_d} precisely for each measured value of $\langle R \rangle$, as grain size and dust content were not sampled exactly at the same depths. Nevertheless, the evolutions of $\langle R \rangle$ and R_{Z_d} strongly suggest a major role of particles pinning on grain growth in polar ice. During interglacial periods such as the Holocene, the dust particle density is too low to have a strong effect on grain growth, as illustrated by R_{Z_d} values much larger than $\langle R \rangle$. During glacial maxima (i.e., stage 2.2, 4.2 and 6.2), at depths where the dust concentration is particularly high, the agreement between R_{Z_d} and $\langle R \rangle$ is striking: the grain size has reached the limiting size imposed by particles pinning. This is in agreement with previous studies made on other ice cores [*Fisher and Koerner*, 1986; *Gow et al.*, 1997; *Jun et al.*, 1998].

[63] It is worth noting that if particles were located randomly within the volume, the R_{Z_d} values would be much larger than the observed grain sizes, even for the largest continental dust concentrations measured along the core (e.g., R_{Z_d} around 500 mm at a depth of 500 m). This led *Alley et al.* [1986b] to conclude that particles pinning could not significantly affect grain growth. We note however that observed grain sizes $\langle R \rangle$ are slightly larger than R_{Z_d} for stage 6.2 (around 1750 m). As discussed in section 2.3.2, this might be explained by partial unpinning of GB from particles for deep, old ice.

[64] This mechanism is also in agreement with other observations:

[65] 1. As detailed in section 2.3.2, Zener pinning narrows the normalized distribution of grain sizes and modifies the mean. This is in full agreement with the profiles shown in Figures 2b and 2c. No other mechanism could easily explain these modifications of the distribution. Moreover, the microstructures observed for volcanic ash layers (black dots in Figures 2a, 2b, and 2c) show the same trends as ice containing a large amount of continental dust: small grain sizes, narrow normalized distributions and smaller mean. The pinning effect of particles is the same whatever their origin, aeolian or volcanic ash [*Gow and Williamson*, 1976].

[66] 2. Despite a significant decrease of temperature, ACR was characterized by a limited increase of the dust content [*Delmonte et al.*, 2002]. As the pinning effect of particles on grain growth is strongly non linear, the limiting grain size values R_{Z_d} are very similar during ACR and Holocene. Consequently, the dust particles density is too low to have a strong effect on grain growth. This explains why the ACR is not revealed by the grain size profile. On the other hand, the well-marked decrease of grain size observed at the stage 3.3 to stage 4.2 transition is easily explained by a simultaneous large change of dust amount.

[67] 3. More evidence comes from continuous grain size analyses. A good example is shown in Figure 12. Figure 12 shows the grain size profile from 339.35 m to 339.65 m, corresponding to an age of about 11200 BP (Figure 12a), along with the corresponding profiles for the dust content (Figure 12b) and for SO_4^{2-} [*Traversi et al.*, 2002] (Figure 12c). Between 339.45 and 339.55 m, a layer of very small grain size is observed. This layer is linked to large values of the dust content resulting from volcanic deposition. Such observations are reported for other sites (e.g., *Gow and Williamson* [1976] for the Byrd core).

[68] The volcanic origin of the dust is attested by a larger average particle size compared to continental dust. On the contrary, small grain sizes are not related to any remarkable features of the soluble impurity records. As an example, larger values of SO_4^{2-} are observed 7 cm above the small grain layer, that is, about 2 years later (Figure 12c). This observation can be explained by a deposition of sulfates few years after the eruption as a result of a stratospheric pathway [*Herron*, 1982], whereas ashes deposition closely follows the eruption [*Legrand and Delmas*, 1987]. We have verified with another continuous grain size analysis performed between 389.0 and 389.6 m that concentrations of sulfates up to 700 $\mu g l^{-1}$ (at 389.45 m), do not affect grain growth.

[69] Adding the effect of all the pinning objects (bubbles, clathrates and dust particles), our model is able to accurately reproduce the observed profile down to about 60 kyr ($\sim$1000 m), in terms of its general trend as well as local fluctuations (see Figure 10c). However, below 1000 m, we

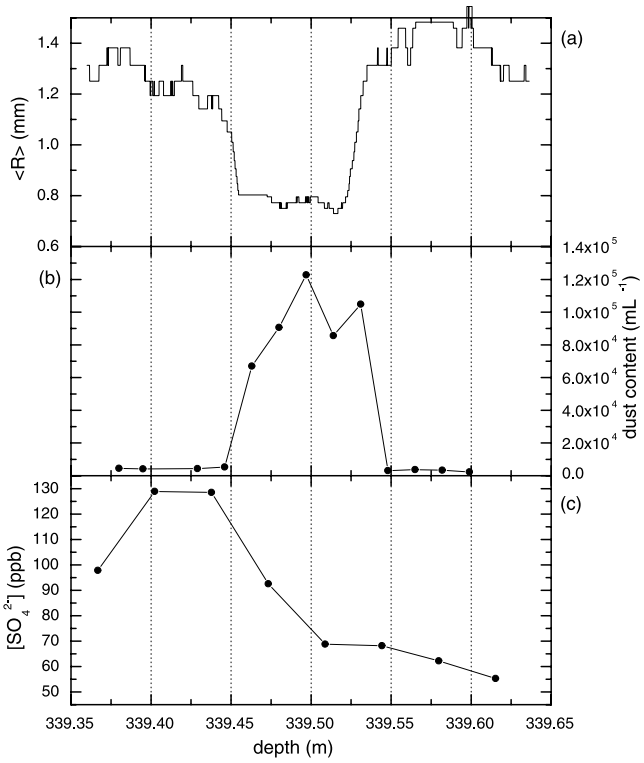

Figure 12. Continuous analysis from 339.35 to 339.65 m corresponding to a volcanic ash layer. (a) Grain size $\langle R \rangle$ measured from linear intercept. (b) Dust content (number of particles). (c) SO_4^{2-} concentration [*Traversi et al.*, 2002].

observed two problems: (1) the simulation overestimates $\langle R \rangle$ down to termination III at 1750 m, but (2) it underestimates $\langle R \rangle$ below. Observation 1 can be explained by the effect of rotation recrystallization, as shown by our model. The model results also suggest a new process in polar ice: the unpinning of dust particles which could explain observation 2. These points are detailed in sections 5.6 and 5.7, respectively.

5.6. Other Recrystallization Processes

[70] As briefly discussed in the introduction, deformation-induced recrystallization mechanisms modify the polar ice microstructure. Migration recrystallization is unlikely to occur along the EPICA Dome C ice core in the depth range analyzed here (100–2200 m), as the temperatures are much lower than −10°C. Data shown in Figure 2a clearly demonstrate that rotation recrystallization is unable to fully balance normal grain growth. In this respect, the EPICA Dome C ice core differs from the Greenland ice cores (GRIP, GISP2) or the Byrd ice core, but resembles the Vostok ice core. This, however, does not mean that rotation recrystallization does not occur. The most efficient way to detect rotation recrystallization is based on the correlation of *c* axes orientation between neighboring grains [*Wilen et al.*, 2003]. This analysis requires detailed crystallographic data that are not yet available for the EPICA ice core. However, rotation recrystallization could be revealed from the microstructure through a modification of the distribution of the angles between GB at triple junctions (on 2D sections) [*Weygand*, 1998]. Without rotation recrystallization, this distribution is strongly centered around 120°. Rotation recrystallization increases the standard deviation of the distribution of angles, σ_θ. A significant increase of about 4° of σ_θ has been observed on the EPICA Dome C ice core within the depth range 800–1500 m (not shown). This can be attributed to the onset of rotation recrystallization, although the flattening of the grains with increasing deformation may partly explain this observation.

[71] The implementation of the rotation recrystallization process into the model followed the dislocation density-based modeling framework proposed by *Montagnat and Duval* [2000]. It is worth noting that this implementation does not introduce any additional adjustable parameters, as the parameters are set to the value proposed by *Montagnat and Duval* [2000] on the GRIP ice core. The model calculates the depth at which the rotation recrystallization appears, z_c, as well as ρ_c, the dislocation density at z_c (see section 2.4 and *Durand* [2004]).

[72] The model indicates that the rotation recrystallization appears at a depth $z_c = 610$ m and a dislocation density $\rho_c = 1.9 \times 10^{11}$ m^{-2}. Recrystallized layers are intercalated between not recrystallized layers within the depth range 610–700 m. Note that the impact of the rotation recrystallization on the grain growth rate is very small within this depth range. Below 700 m, all the layers have reached their ρ_c ($\sim 1.1 \times 10^{11}$ m^{-2} at 700 m); that is, rotation recrystallization is occurring whatever z between 700 and 2135 m. This is in agreement with the standard deviation of the triple junction angles, $\sigma\theta$, which increases from about 800 m (data not shown). The dislocation densities ρ calculated with our model (5×10^{10} m$^{-2} \leq \rho \leq 2 \times 10^{11}$ m^{-2}), are in agreement with the estimation of *De La Chapelle et al.* [1998] for the Vostok ice core ($\rho \sim 1.3 \times 10^{11}$ m^{-2} at a depth of 1000 m).

[73] We compared two different simulated profiles (Figure 13), with and without taking the rotation recrystallization into account (the profile without rotation recrystallization was already shown in Figure 10c). Although the rotation recrystallization is not strong enough to balance the normal grain growth, it significantly decreases the grain size in the depth range 1000–1750 m. On the other hand, the rotation recrystallization does not significantly decrease R over the depths where R is closed to R_Z (stages 4.2 and 6.2). In that case the complex combination of different feedbacks between pinning and rotation recrystallization effects leads to a rapid growth of grains after their subdivision. In other words, the grain size decrease induced by rotation recrystallization is quickly balanced by a rapid grain growth allowed by the relaxation of the pinning pressure P_Z (indeed, the new boundaries are not pinned). Therefore R reaches quickly its previous value near R_Z.

[74] The quantitative agreement between the profile simulated with rotation recrystallization and the data down to 1750 m is particularly striking, as the rotation recrystallization process does not introduce any adjustable parameter into the model. The comparison of the present case with the GRIP core is enlightening. For the GRIP core, the strain rates are much larger. This induces larger recrystallization rates which are able to balance normal grain growth over the range 500–1500 m [*Thorsteinsson et al.*, 1997]. This recrystallization rate can be expressed as the time needed to subdivide each grain into two parts. *Castelnau et al.*

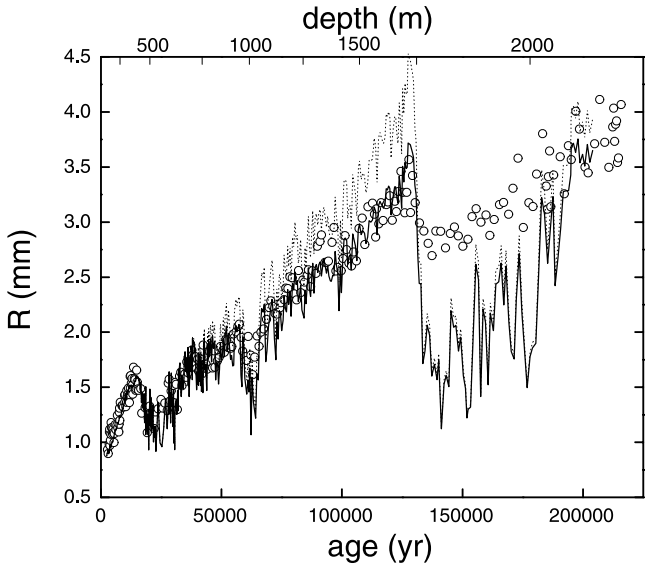

Figure 13. Effect of the rotation recrystallization on the grain size evolution. The dotted line shows the simulation previously shown in Figure 10c, without rotation recrystallization. The solid line represents the introduction of the rotation recrystallization.

[1996] estimated this time to be about 2000 years for the GRIP core whereas we obtained much larger values between 12,000 and 20,000 years for the Dome C ice core.

5.7. Unpinning

[75] As shown in Figure 13, the present model, taking into account the evolution of temperature, the pinning effect of dust particles, bubbles and clathrates, as well as the rotation recrystallization, can accurately reproduce the measurements down to 1750 m. Below this depth, the model significantly underestimates $\langle R \rangle$. We have shown in Figure 11 that the predicted limiting grain size induced by the dust particles R_{Z_d} is smaller than $\langle R \rangle$ within the depth range 1750–2000 m. To remove this paradox, an additional process has to be introduced, namely the unpinning of grain boundaries from the dust particles. So far, we neglected this process, assuming that a pinned microstructure was frozen in its evolution. However, observations performed on the Vostok ice core and shown in Figure 6 indicate that the proportion of bubbles and clathrates located along the grain boundaries decreased with increasing depth. This can be explained only by an unpinning of GB from bubbles and clathrates. This unpinning of GB from bubbles and clathrates is already taken into account in the model through the evolution of the location of these objects summarized in Figure 6. Such observations are not available for the dust particles.

[76] Here, we follow equation (7), initially proposed by *Gore et al.* [1989], to model unpinning from dust particles. We recall that initially $p_{ran} = 0$ and $p_{gb} = 1$. The value of ν_0 and E_U in equation (7) are totally unknown for ice. Therefore we chose to set E_U to the self-diffusion energy, $E_U = 59.8$ kJ.mol^{-1}.

[77] Figure 14 compares the measured evolution of $\langle R \rangle$ with two simulations, (1) without unpinning (i.e., the profile shown in Figure 13) and (2) with unpinning of GB from dust particles with $\nu_0 = 4 \times 10^8$ yr^{-1}. The agreement is surprisingly good, as unpinning starts to significantly affect R only from the depth of 1750 m where the previous simulation failed. This suggest that unpinning indeed takes place within polar ice, owing to the very large timescales involved. However, much work remains to be done in order to properly quantify this process. In Figure 14 we also plot the evolution of p_{gb} with depth. For the LGM ice, p_{gb} is very close to 1, in agreement with the X-ray tomography analysis detailed in section 3.2.2. This proportion falls to almost 0 below 2000 m.

6. Conclusions

[78] The grain growth process in cold ice sheets and the effects of impurities have been analyzed on the basis of a detailed study of the microstructure of the Dome Concordia EPICA ice core, in relation with impurity contents (dust and soluble impurities). We reviewed the possible different mechanisms that could explain the correlation between grain size and surface temperature. A memory effect of the surface temperature at the time of deposition or the drag of soluble impurities have been eliminated on the basis of different observations including grain size distribution profiles or continuous grain size analyses. Then, we developed a model that takes into account normal grain growth and rotation recrystallization, as well as the pinning effect of dust particles, bubbles and clathrates. As these recrystallization processes depend on temperature, the evolution of temperature with depth and climate is also taken into account. In the absence of migration recrystallization, normal grain growth is the only mechanism that increases the grain size with time. This increase is counteracted by pinning of grain boundaries on bubbles, clathrates and dust particles, as well as by rotation recrystallization. The relative contributions of these processes acting against normal grain growth are summarized in Figure 15. Partial

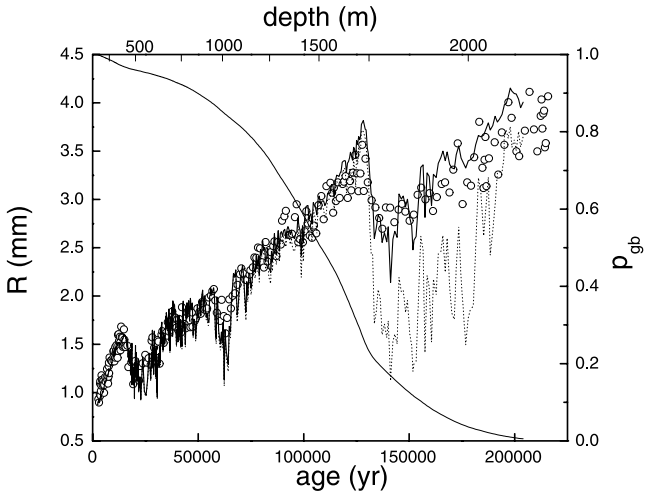

Figure 14. Unpinning effect. The dotted line shows the simulation previously shown in Figure 13 without unpinning. The thick line represents the introduction of the unpinning of GB from dust particles, and the thin line shows the evolution of p_{gb} with depth.

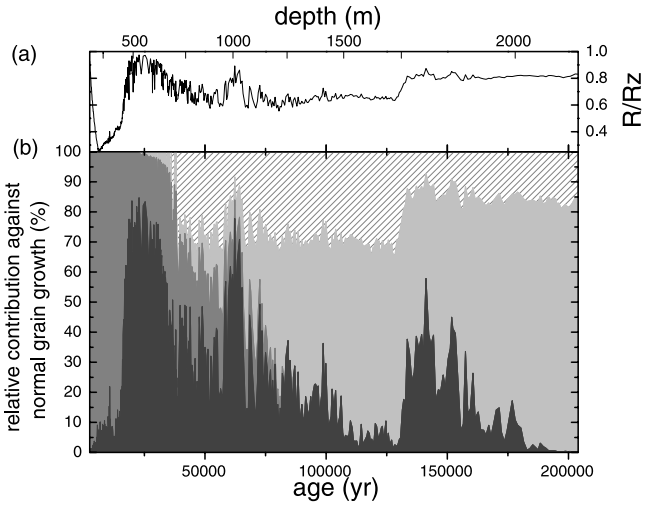

Figure 15. (a) Evolution of the ratio R/R_Z when pinning effects, rotation recrystallization, and unpinning are taken into account. (b) Evolution of the relative contributions of all the effects acting against the normal grain growth: dark gray, contribution of the dust particles pinning; medium gray, contribution of the bubbles pinning; light gray, contribution of the clathrates pinning; hatched area, contribution of the rotation recrystallization.

unpinning of GB from dust particles has also been introduced as a slow thermally activated process.

[79] Our model confirms that the surface temperature changes cannot explain the large grain size decreases observed during glacial to interglacial transitions, in agreement with previous work [*Duval and Lorius*, 1980].

[80] Bubbles and clathrates may explain why an exponent m larger than the theoretical lower bound of 2 (equations (2) and (3)) is observed for grain growth within shallow ice corresponding to Holocene, and could also account for a fraction of the grain size changes observed at climatic transitions (see Figure 15). However, the grain size decreases associated with glacial periods are mainly the result of pinning by dust particles located along GB. Indeed, a X-ray tomography of a LGM ice sample allowed us to locate the largest dust particles which were found to be concentrated along GB. Their pinning effect is therefore much stronger than it would be for a random distribution of particles within the volume. Therefore grain size cannot be considered as a true paleothermometer, but reflects in a complex non linear way of evolution of the dust content, which itself is related to climate changes.

[81] We showed also that clathrates have a significant effect on the grain size in deep ice, and their relative contribution to the restraining force is maximum when the dust content is low (Figure 15). The pinning effect of clathrates cannot be neglected, as the model would overestimate the grain size within these depth ranges if the corresponding pinning force is not taken into account. Taking into account normal grain growth and pinning, the model is able to accurately reproduce the observed grain size profile down to 1000 m (see Figure 10).

[82] As previously shown on other ice cores [*Thorsteinsson et al.*, 1997], rotation recrystallization, which subdivides the grains, counteracts normal grain growth. In Greenland ice core (GRIP, GISP2), rotation recrystallization is strong enough to balance normal grain growth, whereas this is obviously not the case for the Dome C ice core. We estimated the effect of the rotation recrystallization on the average grain size from a modeling framework developed previously [*De La Chapelle et al.*, 1998; *Montagnat and Duval*, 2000]. For the present ice core, the model predicts the onset of the rotation recrystallization at a depth z_c around 610 m (Figure 15). The effect of rotation recrystallization is particularly strong for layers with a low dust content and thus a grain size far from the critical radius (R/R_Z 0.7; see Figure 15). If rotation recrystallization does not fully balance normal grain growth in the present case, it is strong enough to balance the overestimation of R observed in Figure 13. Taking into account rotation recrystallization, our model is able to accurately reproduce the grain size measurements down to 1750 m.

[83] To explain the underestimation of the modeled grain size below 1750 m, we introduced a slow thermally activated unpinning of GB from dust particles, following a theoretical analysis developed for ferrous alloys [*Gore et al.*, 1989]. This allowed to accurately model grain size evolution over the entire depth range 100–2135 m. This unpinning process implies that below 2000 m GB unpinned from most of the particles. However, this analysis of GB unpinning in polar ice remains very preliminary.

[84] Although this analysis is mainly based on a study of the Dome Concordia ice core, the conclusion is certainly relevant for other ice cores within central Antarctica (e.g., the "old" Dome C, Vostok.) that are characterized, as Dome Concordia, by very low surface temperatures and low accumulation rates. On the other hand, the story could be different in places like Greenland. Higher temperatures may change the effectiveness of soluble impurity drag, increase the rate of unpinning and consequently the proportion of dust particles randomly distributed. Finally, the larger accumulation rates imply that the first climatic transition (LGM/Holocene) is observed at depths where other recrystallization processes (induced by viscoplastic deformation, such as rotation recrystallization or migration recrystallization) take place and modify the microstructure. To answer these questions, more detailed analyses of Greenland ice microstructures is required, at a higher sampling frequency, along with X-ray tomography to locate the particles.

[85] Although the average grain size cannot be considered as a true paleothermometer, to understand its evolution with depth and time is of great interest. *Cuffey et al.* [2000] argued that the stain rate of the ice could depend on the grain size. As ice core dating is based on an ice flow model, understanding the deformation history of an ice layer and the possible relations with its microstructure are of primary importance to obtain correct climatic interpretations.

Notation

- α adjustable constant of the pinning strength.
- β coefficient indicating the location of the dislocations within the grains.
- γ grain boundary free energy.
- $\dot{\varepsilon}$ strain rate.
- θ misorientation angle between adjacent subgrains.

θ_c misorientation threshold defining a grain boundary compared to a subboundary.
λ constant used in the calculation of the grain boundary mobility under solute drag.
μ grain boundary mobility.
μ_i intrinsic mobility of the boundary.
ν_0 attempt frequency for unpinning.
ρ dislocation density.
ρ_c threshold dislocation density defining the onset of rotation recrystallization.
σ_θ standard deviation of the angles at the triple junctions.
$\sigma_{\langle R \rangle}$ standard deviation of the mean grain radius.
$\Delta\rho$ dislocation density excess.
c impurity concentration.
c_i concentration of interstitials (point defects).
m experimental grain growth law exponent.
p_U proportion of dust particles leaving a grain boundaries.
p_{gb} proportion of dust particles located along grain boundaries.
p_{ran} proportion of dust particles randomly distributed.
r_d radius of a dust particle.
$\langle r_b \rangle$ average bubble radius.
$\langle r_d \rangle$ average dust particles radius.
t time.
v grain boundary velocity.
z depth (from the surface).
z_c rotation recrystallization starting depth.
$\langle A^{\frac{1}{2}} \rangle$ average of the square root of grain area.
$C(x)$ correlation integral.
E_A activation energy for normal grain growth.
E_f apparent formation energy of interstitials.
E_U activation energy for unpinning.
F_Z pinning force.
K Arrhenius temperature-dependent constant for the theoretical normal grain growth law.
K' Arrhenius temperature-dependent constant for the observed grain growth law.
K_0 grain growth constant.
$\langle L \rangle$ average linear intercept.
N_{ca} number of pairs used in the correlation analysis.
N_b number of bubbles per unit volume of ice.
N_d number of dust particles per unit volume of ice.
N_g number of grains within a thin section.
P driving pressure for grain growth.
P_Z total pinning pressure.
R grain radius calculated by the model.
R^* adimensional parameter.
R_0 initial grain radius.
R_i radius of the grain i (square root of area of the grain i).
R_G perfect gas law constant.
R_Z limiting grain radius.
R_{Z_d} limiting grain radius caused by dust particles.
$\langle R \rangle$ average grain radius (measure).
T temperature.
T_0 surface temperature at the time of deposition.
V_i volume of air inclusions.

[86] **Acknowledgments.** We thank all the EPICA drilling team for their remarkable work on the field and M. Curran for reading the manuscript. This work is a contribution to the "European Project for Ice Coring in Antarctica" (EPICA), a joint European Science Foundation (ESF)/EC scientific program, funded by the European Commission and by national contributions from Belgium, Denmark, France, Germany, Italy, Netherlands, Norway, Sweden, Switzerland. and the United Kingdom. This is EPICA publication 137.

References

Abbruzzese, G., and K. Lucke (1992), Theory of grain growth in the presence of second phase particles, *Mater. Sci. Forum*, *94–96*, 597–604.
Alley, R. B., and G. A. Woods (1996), Impurity influence on normal grain growth in the GISP2 ice core, Greenland, *J. Glaciol.*, *42*, 255–260.
Alley, R. B., J. H. Perepezko, and C. R. Bentley (1986a), Grain growth in polar ice: I. Theory, *J. Glaciol.*, *32*, 415–424.
Alley, R. B., J. H. Perepezko, and C. R. Bentley (1986b), Grain growth in polar ice: II. Appplication, *J. Glaciol.*, *32*, 425–433.
Alley, R. B., J. H. Perepezko, and C. R. Bentley (1988), Long-term climatic changes from crystal growth, *Nature*, *332*, 592–593.
Alley, R. B., A. J. Gow, and D. A. Meese (1995), Mapping *c*-axis fabrics to study physical processes in ice, *J. Glaciol.*, *41*, 197–203.
Anderson, M. P., G. S. Grest, and D. J. Srolovitz (1989), Computer simulation of normal grain growth in three dimensions, *Philos. Mag. B*, *59*, 293–329.
Arnaud, L., J. Weiss, M. Gay, and P. Duval (2000), Shallow ice microstructure at Dome Concordia, Antarctica, *Ann. Glaciol.*, *30*, 8–12.
Barnes, P. R. F., R. Mulvaney, K. Robinson, and E. Wolff (2002), Observations of polar ice from the Holocene and the glacial period using the scanning electron microscope, *Ann. Glaciol.*, *35*, 559–566.
Burke, J. E., and D. Turnbull (1952), Recrystallization and grain growth, *Prog. Metal Phys.*, *3*, 220–292.
Cahn, J. W. (1962), The impurity-drag effect in grain boundary motion, *Acta Metall.*, *10*, 198–789.
Castelnau, O., T. Thorsteinsson, J. Kipfstuhl, P. Duval, and G. R. Canova (1996), Modelling fabric development along the GRIP ice core, central Greenland, *Ann. Glaciol.*, *23*, 194–201.
Cuffey, K. M., T. Thorsteinsson, and E. D. Waddington (2000), A renewed argument for crystal size control of ice sheet strain rates, *J. Geophys. Res.*, *105*, 27,889–27,894.
De La Chapelle, S., O. Castelnau, V. lipenkov, and P. Duval (1998), Dynamic recrystallization and texture development in ice as revealed by the study of deep ice cores in Antarctica and Greenland, *J. Geophys. Res.*, *103*, 5091–5105.
Delmonte, B., J. R. Petit, and V. Maggi (2002), Glacial to Holocene implications of the new 27,000-year dust record from the EPICA Dome C ice core, *Clim. Dyn.*, *18*, 647–660.
Delmonte, B., I. Basile-Doelsch, J. R. Petit, V. Maggi, M. Rolland-Revel, A. Michard, E. Jagoutz, and F. Grousset (2004), Comparing the EPICA and Vostok dust records during the last 220,000 years: Stratigraphical correlation and origin in glacial periods, *Earth Sci. Rev.*, *66*, 63–87.
Durand, G. (2004), Microstructure, recristallisation et déformation des glaces polaires de la carotte EPICA (Dôme Concordia), Antarctique, Ph.D. thesis, Univ. Joseph Fourier–Grenoble I, Grenoble, France. (Available at http://www-lgge.ujf-grenoble.fr/publiscience/theses/these-durand.pdf.)
Durand, G., F. Graner, and J. Weiss (2004), Deformation of grain boundaries in polar ice, *Eur. Phys. Lett.*, *67*, 1038–1044.
Duval, P. (1985), Grain growth and mechanical behaviour of polar ice, *Ann. Glaciol.*, *6*, 79–82.
Duval, P., and O. Castelnau (1995), Dynamic recrystallization of ice in polar ice sheets, *J. Phys.*, *5*, 197–205.
Duval, P., and C. Lorius (1980), Crystal size and climatic record down to the last ice age from Antarctic ice, *Earth Planet. Sci. Lett.*, *48*, 59–64.
EPICA Community Members (2004), Eight glacial cycles from an Antarctic ice core, *Nature*, *429*, 623–628.
Fan, D., S. P. Chen, and L. Q. Chen (1999), Computer simulation of grain growth kinetics with solute drag, *J. Mater. Res.*, *14*, 1113–1123.
Fisher, D. A., and R. M. Koerner (1986), On the special rheological properties of ancient microparticle-laden Northern Hemisphere ice as derived from bore-hole and core measurements, *J. Glaciol.*, *32*, 501–510.
Fukazawa, H., K. Sugiyama, S. Mae, H. Narita, and T. Hondoh (1998), Acid ions at triple junction of Antarctic ice observed by Raman scattering, *Geophys. Res. Lett.*, *25*, 2845–2848.
Gay, M., and J. Weiss (1999), Automatic reconstruction of polycrystalline ice microstructure from image analysis: Application to the EPICA ice core at Dome Concordia, Antarctica, *J. Glaciol.*, *45*, 547–554.
Gore, M. J., M. Grujicic, G. B. Olson, and M. Cohen (1989), Thermally activated grain boundary unpinning, *Acta Metall.*, *37*, 2849–2854.
Gow, A. J. (1968), Bubbles and bubble pressures in Antarctic glacier ice, *J. Glaciol.*, *7*, 167–182.

Gow, A. J. (1969), On the rates of growth of grains and crystals in south polar firn, *J. Glaciol.*, *8*, 241–252.
Gow, A. J., and T. Williamson (1976), Rheological implications of the internal structure and crystal fabrics of the West Antarctic ice sheet as revealed by deep core drilling at Byrd Station, *CRREL Rep. 76-35*, pp. 76–35, Cold Reg. Res. and Eng. Lab., Hanover, N. H.
Gow, A. J., D. A. Meese, R. B. Alley, J. J. Fitzpatrick, S. Anandakrishnan, G. A. Woods, and B. C. Elder (1997), Physical and structural properties of the Greenland Ice Sheet Project 2 ice core: A review, *J. Geophys. Res.*, *102*, 26,559–26,575.
Hammer, C. U. (1977), Past volcanism revealed by Greenland ice sheet impurities, *Nature*, *270*, 482–486.
Herron, M. M. (1982), Impurity soucres of F^-, Cl^-, NO_3^- and SO_4^{2-} in Greenland and Antarctic precipitation, *J. Geophys. Res.*, *87*, 3052–3060.
Higgins, G. T. (1974), Grain-boundary migration and grain growth, *Metal Sci.*, *8*, 142–150.
Hillert, M. (1965), On the theory of normal and abnormal grain growth, *Acta Metall.*, *13*, 227–238.
Humphreys, F. J., and M. Hatherly (1996), *Recrystallization and Related Annealing Phenomena*, Elsevier, New York.
Jacka, T. H., and L. Jun (1994), The steady-state crystal size of deforming ice, *Ann. Glaciol.*, *20*, 13–18.
Jouzel, J., et al. (2001), A new 27 ky high resolution East Antarctic climate record, *Geophys. Res. Lett.*, *28*, 3199–3202.
Jun, L., T. H. Jacka, and V. Morgan (1998), Crystal-size microparticle record in the ice core from Dome Summit South, Law Dome, East Antarctica, *Ann. Galciol.*, *27*, 343–348.
Korvin, G. (1992), *Fractal Models in the Earth Sciences*, Elsevier, New York.
Legrand, M., and R. J. Delmas (1987), A 220-year continuous record of volcanic H_2SO_4 in the Antarctic ice sheet, *Nature*, *327*, 671–676.
Lipenkov, V. Y. (2000), Air bubbles and air-hydrate in the Vostok ice core, in *Physics of Ice Records*, edited by T. Hondo, pp. 327–358, Hokkaido Univ. Press, Sapporo, Japan.
Lücke, K., and K. Detert (1957), A quantitative theory of grain-boundary motion and recrystallization in metals in the presence of impurities, *Acta Metall.*, *5*, 628–637.
Lücke, K., and H. P. Stüwe (1971), On the theory of impurity controlled grain boundary motion, *Acta Metall.*, *19*, 1087–1099.
Montagnat, M., and P. Duval (2000), Rate controlling process in the creep of polar ice, influence of grain boundary migration associated with recrystallization, *Earth Planet. Sci. Lett.*, *183*, 179–186.
Montagnat, M., P. Duval, P. Bastie, B. Hamelin, O. Brissaud, M. de Angelis, J. R. Petit, and V. Y. Lipenkov (2001), High crystalline quality of large single crystals of subglacial ice above Lake Vostok (Antarctica) revealed by hard X-ray diffraction, *C. R. Acad. Sci., Ser. 2*, *333*, 419–425.
Nichols, F. A. (1966), Theory of grain growth in porous compacts, *J. Appl. Phys.*, *37*, 4599–4602.
Paterson, W. S. B. (1994), *The Physics of Glaciers*, Elsevier, New York.
Peix, G., P. Duchauvelle, and N. Freud (2000), *X-Ray Tomography in Materials Science*, Ed. Hermes, Paris.
Petit, J. R., P. Duval, and C. Lorius (1987), Long-term climatic changes indicated by crystal growth in polar ice, *Nature*, *326*, 62–64.
Petit, J. R., P. Duval, and C. Lorius (1988), Long-term climatic changes indicated by crystal growth in polar ice: Reply, *Nature*, *332*, 593.
Petit, J. R., et al. (1999), Climate and atmospheric history of the past 420,000 years from the Vostok ice core, Antarctica, *Nature*, *399*, 429–436.
Ralph, B. (1990), Grain growth, *Mater. Sci. Technol.*, *6*, 1139–1144.
Riege, S. P., C. V. Thompson, and H. J. Frost (1998), The effect of particle-pinning on grain size distributions in 2D simulations of grain growth, in *Grain Growth in Polycrystalline Materials III*, edited by H. Weiland, B. L. Adams, and A. D. Rollet, pp. 295–301, Miner., Metals and Mater. Soc., Warrendale, Pa.
Ritz, C. (1989), Interpretation of the temperature profile measured at Vostok, East Antartica, *Ann. Glaciol.*, *12*, 138–144.
Röthlisberger, R., M. Bigler, M. Hutterli, S. Sommer, B. Stauffer, H. G. Junghans, and D. Wagenbach (2000), Technique for continuous high-resolution analysis of trace substances in firn and ice cores, *Environ. Sci. Technol.*, *34*, 338–342.
Röthlisberger, R., R. Mulvaney, E. W. Wolff, M. A. Hutterli, M. Bigler, S. Sommer, and J. Jouzel (2002), Dust and sea salt variability in central East Antarctica (Dome C) over the last 45 kyrs and its implications for southern high-latitude climate, *Geophys. Res. Lett.*, *29*(20), 1963, doi:10.1029/2002GL015186.
Smith, C. S. (1948), Grains, phases, and interfaces: An interpretation of microstructure, *Trans. Metall. Soc. AIME*, *175*, 15–51.
Song, X., G. Liu, and N. Gu (2000), Simulation of the influence of the quantity of second-phase particles on grain growth, *Z. Metallkd.*, *91*, 227–231.
Steffensen, J. P. (1997), The size distribution of microparticles from selected segments of the GRIP ice core representing different climatic periods, *J. Geophys. Res.*, *102*, 26,755–26,763.
Thorsteinsson, T., J. Kipfsthul, and H. Miller (1997), Textures and fabrics in the GRIP project, *J. Geophys. Res.*, *102*, 26,583–26,599.
Traversi, R., S. Becagli, E. Castellano, A. Migliori, M. Severi, and R. Udisti (2002), High-resolution fast ion chromatography (FIC) measurements of chloride, nitrate and sulfate along the EPICA Dome C ice core, *Ann. Glaciol.*, *35*, 291–298.
Tweed, C. J., N. Hansen, and B. Ralph (1982), Grain growth in samples of aluminium containing alumina particles, *Metall. Trans. A*, *14*, 2235–2243.
Uchida, T., S. Mae, T. Hondoh, P. Duval, and V. Y. Lipenkov (1993), Measurements of surface energy of air-hydrate crystals in Vostok ice core, Antarctica, *NIPR Symp. Polar Meteorol. Glaciol.*, *7*, 1–6.
Underwood, E. E. (1970), *Quantitative Stereology*, Addison-Wesley, Boston, Mass.
Weygand, D. (1998), Simulation numérique de la croissance des grains, Ph.D. thesis, Inst. Natl. Polytech. de Grenoble, Grenoble, France.
Weygand, D., Y. Bréchet, J. Lépinoux, and W. Gust (1998), Three dimensional grain growth: A vertex dynamics simulation, *Philos. Mag. B*, *79*, 703–716.
Wilen, L. A., C. L. Diprinzio, R. B. Alley, and N. Azuma (2003), Development, principles, and applications of automated ice fabric analysers, *Microsc. Res. Tech.*, *62*, 2–18.
Wolff, E. W., R. Mulvaney, and K. Oates (1988), The location of impurities in Antarctic ice, *Ann. Glaciol.*, *11*, 194–197.
Wolff, E. W., I. Basile, J. R. Petit, and J. Schwander (1999), Comparison of Holocene electrical records from Dome C and Vostok, Antarctica, *Ann. Glaciol.*, *29*, 89–93.

J. M. Barnola, B. Delmonte, P. Duval, G. Krinner, F. Parrenin, C. Ritz, and J. Weiss, Laboratoire de Glaciologie et Géophysique de l'Environnement, CNRS and Université Joseph Fourier, F-38402 Saint-Martin-d'Hères Cedex, France. (weiss@lgge.obs.ujf-grenoble.fr)

M. Bigler and G. Durand, Niels Bohr Institute, Rockfeller Komplekset, Juliane Maries Vej 30, DK-2100 Copenhagen, Denmark.

V. Lipenkov, Arctic and Antarctic Research Institute, 38 Bering Str., 199397 St. Petersburg, Russia.

R. Röthlisberger, British Antarctic Survey, High Cross, Madingley Road, CB3 0ET Cambridge, UK.